iScience

CellPress
OPEN ACCESS

Article

Competing excitation paths in luminescent heterobimetallic Ln-Al complexes: Unraveling interactions via experimental and theoretical investigations

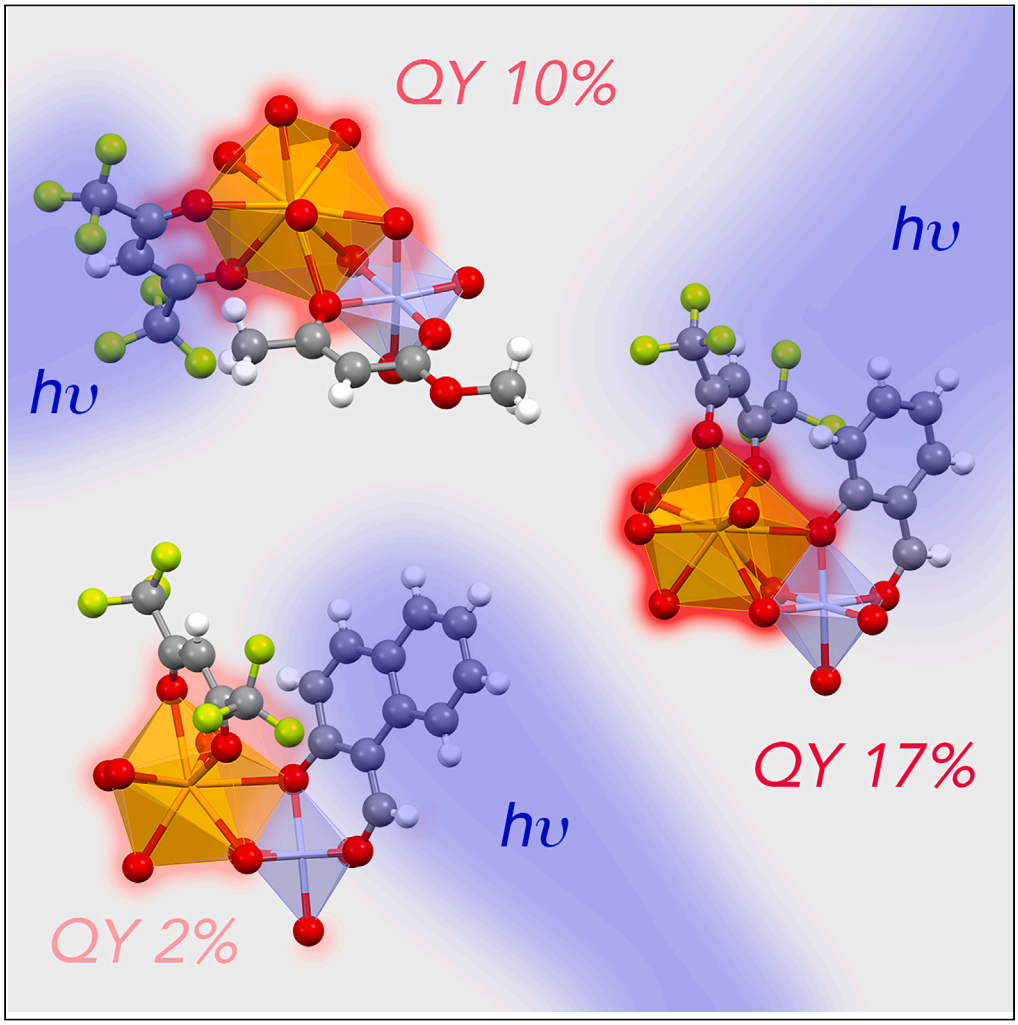

Luca Bellucci, Silvia Carlotto, Gregorio Bottaro, ..., Fabio Marchetti, Simona Samaritani, Lidia Armelao

gregorio.bottaro@cnr.it (G.B.)
luca.labella@unipi.it (L.L.)

Highlights

Synthetic toolbox to access heterobimetallic luminescent Ln^{3+}-Al^{3+} complexes

Emission properties explained with two non-interacting excitation paths

DFT simulated absorption spectra help to rationalize the different excitation paths

Bellucci et al., iScience 26, 106614
May 19, 2023
https://doi.org/10.1016/j.isci.2023.106614

iScience

CellPress
OPEN ACCESS

Article

Competing excitation paths in luminescent heterobimetallic Ln-Al complexes: Unraveling interactions via experimental and theoretical investigations

Luca Bellucci,[1,2] Silvia Carlotto,[1,3] Gregorio Bottaro,[1,5,*] Luca Babetto,[3] Luca Labella,[1,2,*] Elisa Gallo,[2] Fabio Marchetti,[2] Simona Samaritani,[2] and Lidia Armelao[3,4]

SUMMARY

The interest for heterometallic lanthanide-*d* or-*p* metal (Ln-M) complexes is growing because of a potential cooperative or synergistic effect related to the proximity of two different metals in the same molecular architecture affording special tunable physical properties. To exploit the potentiality of Ln-M complexes, suitable synthetic approaches, and the in-depth understanding of the effect of each building block on their properties are mandatory. Here, we report the study on a family of heterometallic luminescent complexes [Ln(hfac)$_3$Al(L)$_3$], Ln= Eu^{3+} and Tb^{3+}. Using different L ligands, we investigated the effect of the steric and electronic properties of the Al(L)$_3$ fragment, highlighting the general validity of the employed synthetic route. A marked difference in the light emission of [Eu(hfac)$_3$Al(L)$_3$] and [Tb(hfac)$_3$ Al(L)$_3$] complexes has been observed. Thanks to photoluminescence experiments and Density Functional Theory calculations, Ln^{3+} emissions are explained with a model involving two non-interacting excitation paths through hfac or Al(L)$_3$ ligands.

INTRODUCTION

The interest for the synthesis and properties of heterometallic lanthanide-*d* or-*p* metal (Ln-M) complexes is continuously growing for their potential use in many fields such as diagnostic medicine[1,2] and biology,[3,4] or for the development of molecular switches,[5] magnetic[6–8] and luminescent materials.[9–11]

Heterometallic Ln-M compounds can be obtained through different synthetic procedures exploiting the marked preference of lanthanide ions toward oxygen donor ligands,[12–14] their considerably larger ionic radius,[15,16] or both.[17] A simpler and more attractive route involves the reaction between a mononuclear *d* or *p* metal complex featuring Lewis basic sites and either a formally coordinatively unsaturated lanthanide fragment,[18] or a lanthanide complex having labile donors in the coordination sphere.[19] For this reaction, the [Ln(hfac)$_3$] fragment, where hfac is hexafluoroacetylacetonato (a β-diketonato ligand), has been commonly chosen because fluorinated groups make the lanthanide center susceptible to attack even by relatively weak bases. This route has been used for dipositive (M^{2+}= Cu^{2+})[20,21] and tripositive (M^{3+}= Cr^{3+}, Fe^{3+}, Ga^{3+}, and Co^{3+})[18,19,22,23] metal complexes mainly for magnetic studies. For square planar or square pyramidal[20,21] copper(II) mononuclear complexes with acetylacetonato (acac) and salen ligands, two oxygen atoms on the same side of the square base are able to coordinate the lanthanide center (Figure 1A). Conversely, for octahedral tripositive metal mononuclear complexes (M),[18] a few reported examples show only acetylacetonato ligands, with three donor atoms from three different acac ligands, lying on the same triangular face and bridging the two metal ions (Figure 1B).

Synthetic access to the heterometallic compounds is related to an excess of electron density on the acac ligands leading to a stable Lewis acid/Lewis base adduct. Scrambling of ligands, always possible in the synthesis of heterometallic complexes,[24] was not noticed. Our interest in the development of luminescent complexes[25–30] has led us to consider the possibility to prepare luminescent heterometallic compounds using this synthetic route. In this work we report the synthesis and the photoluminescence studies of a series of heterometallic Ln-Al complexes with composition [Ln(hfac)$_3$Al(L)$_3$] (where

[1]CNR ICMATE and INSTM, Dipartimento di Scienze Chimiche, Università di Padova, via Marzolo 1, 35131 Padova, Italy

[2]Dipartimento di Chimica e Chimica Industriale and CIRCC, Università di Pisa, via Giuseppe Moruzzi 13, 56124 Pisa, Italy

[3]Dipartimento di Scienze Chimiche and INSTM, Università di Padova, via Marzolo 1, 35131 Padova, Italy

[4]Dipartimento di Scienze Chimiche e Tecnologie dei Materiali (DSCTM) Consiglio Nazionale delle Ricerche Piazzale A. Moro 7, 00185 Roma, Italy

[5]Lead contact

*Correspondence: gregorio.bottaro@cnr.it (G.B.), luca.labella@unipi.it (L.L.)

https://doi.org/10.1016/j.isci.2023.106614

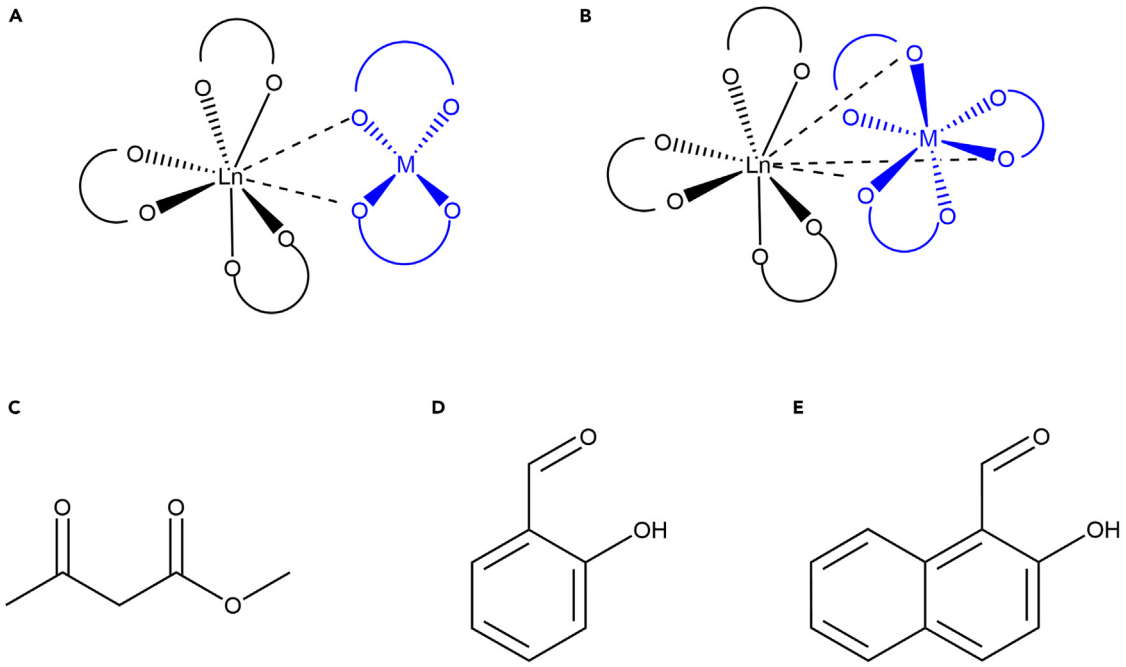

Figure 1. Exemplification of the donor atoms bridging the [Ln(hfac)$_3$] moiety

(A and B) Exemplification of the donor atoms bridging the [Ln(hfac)$_3$] moiety (in black) in case of (A) a square planar or square based pyramidal geometry and (B) an octahedral geometry for the M center (in blue).

(C and D) Schematic representation of the L ligands used in this work. (C) methyl acetoacetate, (D) salicylaldehyde, and (E) 2-hydroxynaphthaldehyde.

Ln^{3+}= Eu^{3+}, Gd^{3+}, and Tb^{3+} and HL = methyl acetoacetate, Hmeac; salicylaldehyde, Hsal; and 2-hydroxynaphthaldehyde, Hnaphthal; Figures 1 C, D and E), as well as DFT-based theoretical studies to investigate the electronic properties[31–33] *i.e.*, the oxygen nucleophilicity and the absorption spectra in these systems. Europium and terbium have been chosen because of their characteristic emission. We focused the attention on Al^{3+} because it forms easily accessible octahedral mononuclear complexes with chelate oxygen donors ligands[34–36] potentially useful for the synthesis of heterometallic complexes. Moreover, thanks to its low lability ($k_{H_2O} \approx 1\ s^{-1}$),[37] Al^{3+} should help minimizing ligand scrambling. Noteworthy, a few europium aluminum complexes have been studied for their photoluminescence properties.[38–40]

The possibility of varying the oxygen donor chelate ligands on the Al center in octahedral geometry appeared an easy way to have access to a family of complexes with tunable luminescent properties. In this regard, the in-depth understanding of the effect of each building block on the emission properties is crucial, not only to maximize the brightness of the emitters but also to identify the more suitable molecular fragment for further functionalization to achieve synthetic flexibility without compromising the emission properties. We studied the absorption and emission properties of the powder samples finding marked differences within the family both varying L ligand and the emitting Ln^{3+} ion. DFT calculation helped rationalize the experimental evidence that can be well described with a model consisting of two non-interacting excitation paths going through hfac ligands or Al(L)$_3$ moieties.

RESULTS AND DISCUSSION

Synthesis, structural data, geometrical parameters and acidity properties

The reaction between anhydrous [Ln(hfac)$_3$] and [Al(meac)$_3$] has been carried out under nitrogen in toluene at room temperature using a 1:1 reaction stoichiometry obtaining products with analytical compositions [Ln(hfac)$_3$Al(meac)$_3$] (**1Eu** for Ln^{3+}= Eu^{3+} and **1Gd** for Ln^{3+}= Gd^{3+}) in moderate to good yields, Scheme 1.

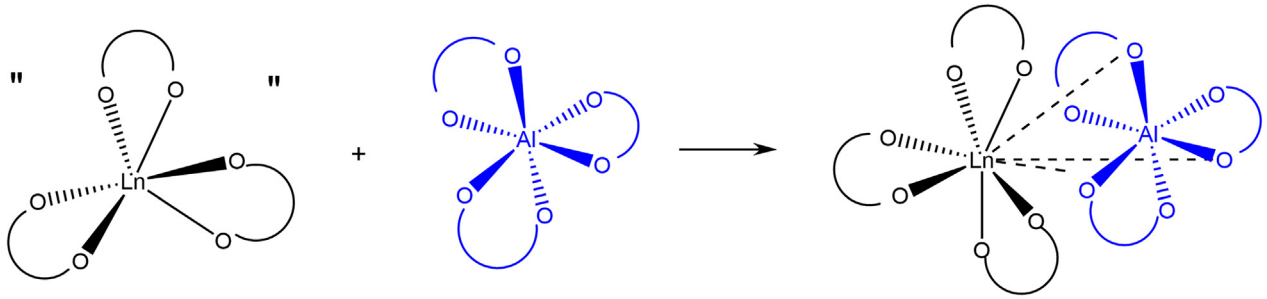

H– = hexafluoroacetylacetone (H-hfac)

H– = methyl acetoacetate (H-meac)
salycylaldehyde (H-sal)
2-hydroxynaphthaldehyde (H-naphthal)

Ln = Eu, Gd, Tb

Quotation marks indicate a formal unsaturated fragment

Scheme 1. General reaction scheme for heterobimetallic complexes

General reaction scheme for heterobimetallic complexes synthesis, showing stoichiometry and product backbone.

The products show superimposable IR spectra not changing for short time air expositions. The molecular structure of **1Eu**, determined by X-ray diffraction analysis on single crystals obtained from a heptane solution cooled at −20 °C, confirmed the composition of the complex.

The structure of **1Eu** (Figure 2A) is characterized by a dinuclear unit in which the europium center shows a coordination number (CN) of 9 and a tricapped-trigonal-prismatic coordination geometry sharing the trigonal face (O7, O10, and O13 in Figure 2A) with the aluminum octahedron. The coordination of the $[Al(meac)_3]$ moiety to the europium center occurs through 3 bridging oxygen atoms (μ_2-O) of the 3 O=C-CH_3 fragments of the meac ligands. The coordination of the carbonyl CO is preferred to that of the ester carbonyl group and this behavior can be explained by considering the Lewis basicity of the two oxygen atoms.

To investigate this aspect, the Fukui function for the Al^{3+} complex was calculated exploiting DFT numerical experiments. This function reflects the reactivity of a site, the capability of the molecule to lose or accept an

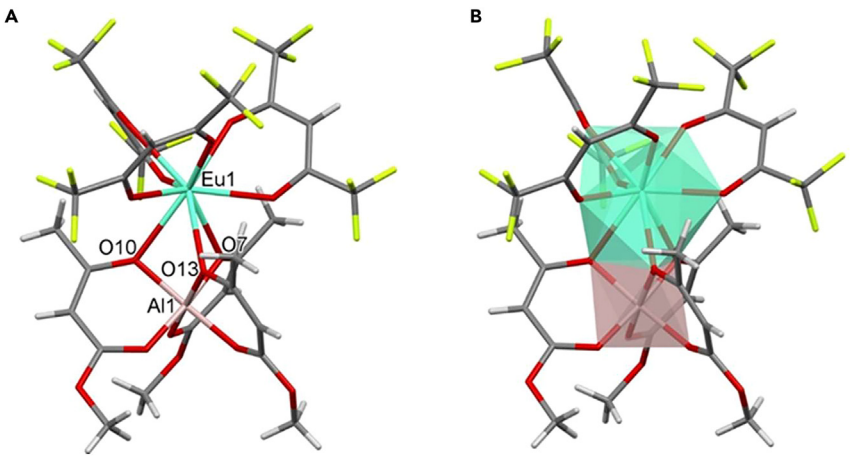

Figure 2. Molecular structure and coordination polyhedral of 1Eu

(A) Molecular structure of **1Eu**$[Eu(hfac)_3Al(meac)_3]$.

(B) Metal centers coordination polyhedra.

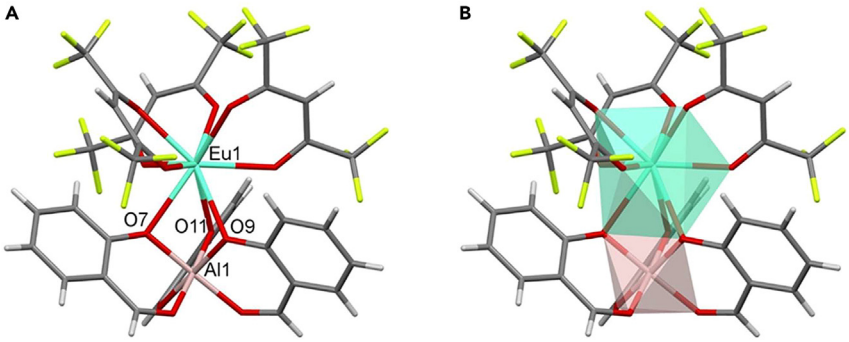

Figure 3. Molecular structure and coordination polyhedral of 2Eu

(A) Molecular structure of **2Eu**[Eu(hfac)$_3$Al(sal)$_3$].

(B) Metal centers coordination polyhedra.

electron, which can be immediately identified with the nucleophilic or electrophilic character of a molecule (see computational details for additional information). The atomic contributions to the Fukui function are based on a Mulliken population analysis. DFT calculations of the condensed Fukui function for the nucleophilicity (f_k^-) of the [Al(meac)$_3$] complex indicate that the oxygen in the O=C-CH$_3$ group is more nucleophilic (higher Lewis basicity) than the O=C-OCH$_3$ one (f_k^- = 0.036 for the former and f_k^- = 0.017 for the latter) and is therefore expected to bridge the two metal ions. Owing to the similar spatial footprint of the O=C-CH$_3$ and O=C-OCH$_3$ groups, the steric factors are expected to play only a marginal role. Although the aluminum precursor is a mixture of the two geometric isomers[35] only the *fac*-isomer of [Al(meac)$_3$] is coordinated to europium in the structure of **1Eu**, and this is also consistent with the higher nucleophilicity of oxygen atom in O=C-CH$_3$ group obtained from the DFT calculations. **1Gd** has been similarly crystallized and resulted isotypic with **1Eu**. NMR studies (see supplemental information) performed on **1Eu** showed that the complex is also stable in solution and no evidence of the presence of the two separate building blocks was detected. Furthermore, also in solution, a single molecular compound with *fac*-[Al(meac)$_3$] coordinated to the europium fragment is present, and no ligand scrambling has been observed for short time periods.

In the attempt to modify the steric and electronic properties of the aluminum complex, the known salicylate complex [Al(sal)$_3$],[34] a mononuclear complex with the metal center in octahedral geometry has been considered. Examples of salicylate ligands bridging *d* transition metals and lanthanide ions have been already reported in the literature,[41–44] as well as luminescent lanthanide complexes based on salicylate ligands.[45–48] The reaction of [Ln(hfac)$_3$] with [Al(sal)$_3$] was carried out in anhydrous toluene with a 1:1 reaction stoichiometry recovering a yellow solid with analytical composition [Ln(hfac)$_3$Al(sal)$_3$] (**2Eu** for Ln^{3+}= Eu^{3+} and **2Gd** for Ln^{3+}= Gd^{3+}) in good yields, Scheme 1 NMR spectra for **2Eu** support the formation of a single heterometallic compound. Single crystals suitable for X-ray diffraction studies were obtained cooling a hot heptane solution of **2Eu** whose molecular structure is represented in Figure 3A.

As in the previous case, the europium center has CN 9 and a tricapped-trigonal-prismatic coordination geometry sharing the trigonal face (O7, O9, and O11 in Figure 3A) with the aluminum octahedron (Figure 3B). The 3 salicylate ligands of the *fac*-isomer of [Al(sal)$_3$] are bridging the two metal ions through the phenolate oxygen atom. Analogous calculations to those presented above for [Al(meac)$_3$] were carried out and identical considerations can be made based on the condensed Fukui function: the oxygen with the largest nucleophilic character (*i.e.* the stronger Lewis base) is the one which ultimately bridges the metals: f_k^- = 0.029 for the bridge oxygen versus f_k^- = 0.015 for the other. The gadolinium derivative [Gd(hfac)$_3$Al(sal)$_3$] (**2Gd**) resulted isostructural to **2Eu**.

The use of a [Al(L)$_3$] moiety containing an L ligand with a higher aromaticity was expected to shift the absorption spectra of the heterometallic complex toward the visible range. For this reason, the Hnaphthal ligand was chosen. The complex [Al(naphthal)$_3$], not previously reported in the literature has been prepared in this work for protonolysis of the commercial aluminum tert-butoxide complex. (see supplemental information) The new compound, structurally characterized, is a mononuclear octahedral complex (see

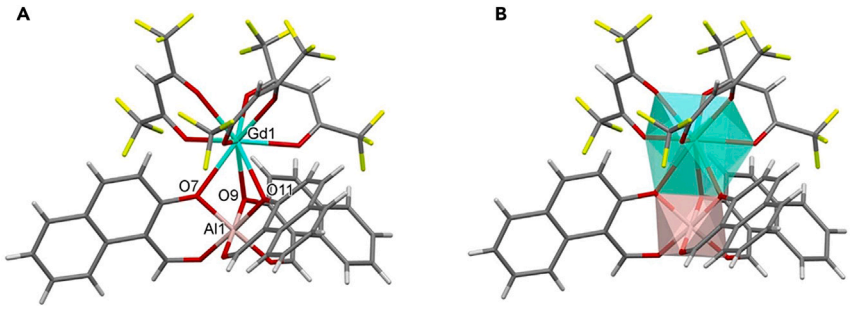

Figure 4. Molecular structure and coordination polyhedral of 3Gd

(A) Molecular structure of **3Gd**[Gd(hfac)$_3$Al(naphthal)$_3$].

(B) Metal centers coordination polyhedra.

supplemental information), suitable for the heterometallic synthesis. The reaction between equimolar amounts of [Ln(hfac)$_3$] and [Al(naphthal)$_3$] compounds in anhydrous toluene led to products with composition [Ln(hfac)$_3$Al(naphthal)$_3$] (**3Eu** for Ln^{3+}= Eu^{3+} and **3Gd** for Ln^{3+}= Gd^{3+}), Scheme 1. NMR spectra for **3Eu** support the formation of a single heterometallic compound. Single crystals suitable for structure determination through X-ray diffraction analysis were obtained for compound **3Gd** after cooling a heptane solution at −20 °C (Figure 4).

The structure of **3Gd** is analogue to **2Eu** with a nona-coordinated gadolinium center in a trigonal tricapped prismatic geometry with 3 hydroxyl oxygen atoms of the aluminum moiety bridging the two metal centers. Once again, calculation of the Fukui function for the [Al(naphthal)$_3$] complex allows us to identify the more nucleophilic oxygen (f_k^- = 0.018 versus f_k^- = 0.016) and correctly predicts which one ends up bridging the two ions. This time, however, the differences are not as large as in the other two cases. To evaluate whether this small difference could differentiate the two oxygens for their Lewis character, the relative stability of the two complexes, featuring the naphthal ligand bridging the two metal ions with either oxygen atom, was evaluated considering the difference in energy of the two forms (resulting from geometry optimizations). The form with the hydroxyl oxygen bridging the two metal ions is 5.45 kcal/mol more stable than the alternative form, which at room temperature would result in a 99.99% fraction of the most stable isomer considering a Boltzmann distribution. X-ray studies on single crystals of **3Eu** resulted to have the same crystalline phase of **3Gd**.

The relative Brønsted base character of the two oxygen atoms in each ligand was also evaluated, to see whether it correlates with the relative strength as Lewis bases. A thorough and quantitative evaluation of the Brønsted base strength would involve calculating the relative energy of the neutral and deprotonated forms in water, taking into account the contribution of the free proton as well, which is not straightforward. However, it is possible to evaluate the relative base character of these two oxygens simply by optimizing the geometry of the two forms in which either oxygen bears the hydrogen atom. For all three ligands, starting from the geometry in which the less nucleophilic oxygen atom bears the proton, the optimization inevitably converges to the geometry in which the proton is transferred to the more nucleophilic one, clearly indicating that the latter is also a much stronger Brønsted base.

To quantify the relative energies of these two forms, a constrained geometry optimization was carried out, in which the proton is fixed at the O-H distance seen in the other form. For meac, sal, and naphthal, the less stable form was found to be 8.67, 11.98, and 6.80 kcal/mol higher in energy than the more stable one, respectively. The Brønsted and Lewis character of different species cannot be correlated rigorously in principle, but for this specific situation it might be worth evaluating in case one is interested in a rapid pre-screening of a series of ligands and only wants to individuate which side the ligand is more likely to place itself as a bridge, as these are very simple and quick calculations on the isolated ligand molecules.

Terbium analogues have been prepared for comparison purposes of their luminescent properties. Reacting [Tb(hfac)$_3$] with [Al(meac)$_3$],[Al(sal)$_3$], and [Al(naphthal)$_3$] in anhydrous toluene, [Tb(hfac)$_3$Al(meac)$_3$]

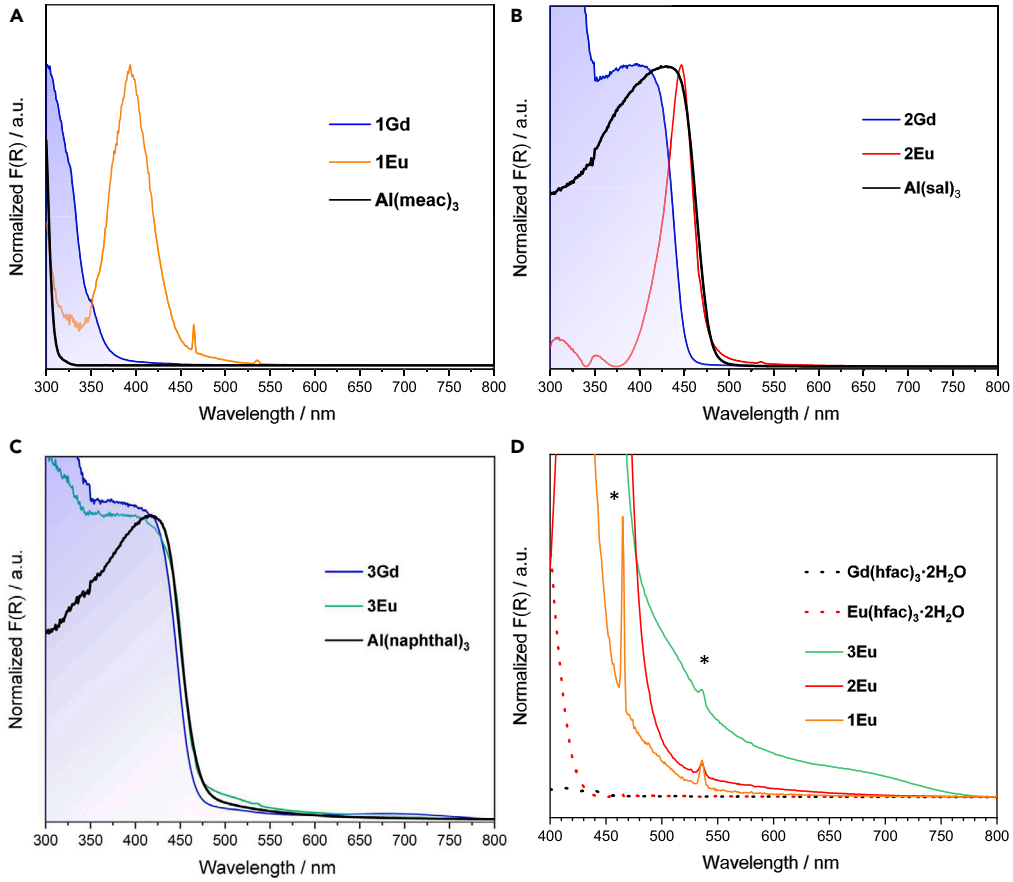

Figure 5. Diffuse reflectance spectra of samples powders

(A–D) Diffuse reflectance spectra of samples powders of $[Eu(hfac)_3Al(L)_3]$ and $[Gd(hfac)_3Al(L)_3]$ complexes. (A) L = meac, (B) L = sal, and (C) L = naphthal. The blue-filled regions highlight the absorption of Gd^{3+}-containing compounds. (D) Overlap of low-energy tails of the absorption spectra. The narrow bands starred in panel (D) are the $^5D_2 \leftarrow {}^7F_0$ and $^5D_1 \leftarrow {}^7F_1$ transitions of Eu^{3+} ions.

(**1Tb**), $[Tb(hfac)_3Al(sal)_3]$ (**2Tb**), and $[Tb(hfac)_3Al(naphthal)_3]$ (**3Tb**) have been obtained in good yields (Scheme 1) with IR spectra superimposable with those of the corresponding europium and gadolinium analogues.

Absorption and emission spectra

We developed a family of hetero-bimetallic complexes in which the $Ln(hfac)_3$ unit is kept constant whereas the ligands of $Al(L)_3$ fragments have increasing aromaticity. This choice allowed us to study the effect of the steric and electronic properties of the $Al(L)_3$ building block on the solid-state absorption and emission of the $[Ln(hfac)_3Al(L)_3]$ complexes.

Concerning the solid-state absorption spectra (Figure 5), besides ligand- (LC) and metal-centered (MC) bands, charge transfer transitions (CT) are often observed. Intrashell 4f-4f transitions, because of their peculiar narrow and structured bandshape, are easy to identify. However, the attribution of LC and CT contribution can be challenging. The presence of the latter is generally revealed by comparing the absorption spectra of Eu^{3+} complexes with those of the corresponding Gd^{3+} compounds (Figures 5 and S7) for which low-energy CTs (<25000 cm^{-1}), fundamental in the determination of the emission properties of Eu^{3+},[49,50] are not possible. The Gd^{3+} first excited state lays *ca.* 32000 cm^{-1} above the ground state. Thus, to attribute the transitions in the spectra of heterometallic complexes, the comparison with the absorption profiles of $[Eu(hfac)_3Al(L)_3]$, and $[Gd(hfac)_3Al(L)_3]$ complexes, and of the $Al(L)_3$ fragments is necessary.

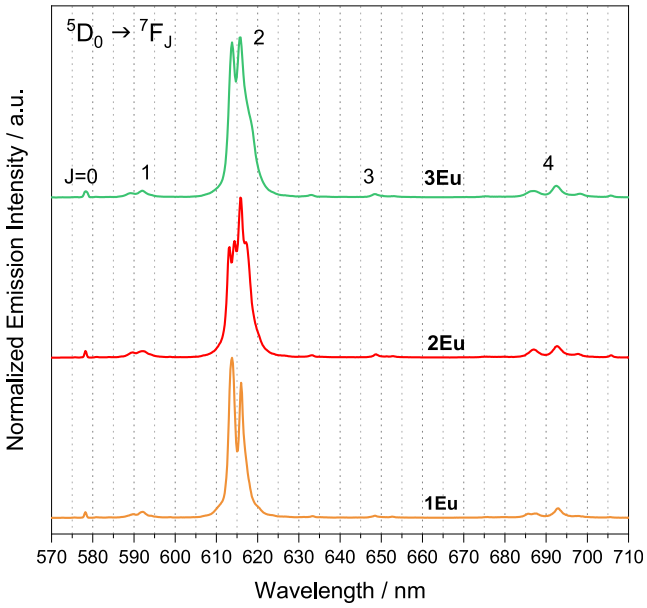

Figure 6. Emission spectra for samples 1Eu, 2Eu, and 3Eu

Emission spectra for samples**1Eu**, **2Eu**, and **3Eu** excited at 370 nm.

The absorption spectrum of **1Eu** (Figure 5A) is characterized by a symmetric band centered at 395 nm that is attributed to ligand to metal (LM) CT transitions being located where **1Gd** and Al(meac)$_3$ do not show absorptions. The shape of the **2Eu** spectrum (Figure 5B), containing an aromatic moiety, is similar to those of **1Eu**, but is red-shifted by 50 nm. The partial overlap between the spectra of **2Eu**, and Al(sal)$_3$ does not allow a clear attribution. The band is likely to be composed of both LC and LMCT transitions. A clue for the latter is the low energy tail at $\lambda > 500$ nm not present in the spectra of **2Gd**. In **3Eu** and **3Gd**, to further increase the π delocalization on L, we used 2-hydroxynaphthaldehyde, resulting in broader absorption spectra (Figure 5C). Absorptions at wavelengths longer than 500 nm are observed as well. As for **2Eu**, the contribution of both LC and LMCT transitions are present. Of note, although for **1Eu** and **2Eu** the absorption spectra are quite different from those of their building blocks, the spectra of **3Eu** and Al(naphthal)$_3$ are almost superimposable. Figure 5D highlights the region at $\lambda > 400$ nm ($E < 25000$ cm^{-1}) to show the effects of the different Al(L)$_3$ moieties in this important spectral region, where Eu^{3+} excited states involved in the sensitized emission process are located. In the absorption spectrum of **1Eu**, the $^5D_2 \leftarrow {}^7F_0$ (465 nm) and $^5D_1 \leftarrow {}^7F_1$ (536 nm) transitions of Eu^{3+}ions are visible whereas for **2Eu** and **3Eu** only the latter, though strongly overlapped with the tails of LMCT/LC, is observed. These features affect the emission properties of the complexes.

The emission spectra in Figure 6 show the Eu^{3+} characteristic bands from the $^5D_0$ excited state to the ground state multiplets ^7F_J J = 0, 1, 2, 3, and 4.[51,52] The presence of the $^5D_0 \rightarrow {}^7F_0$ and the high relative intensity of the $^5D_0 \rightarrow {}^7F_2$ transitions respect to those of the other ^7F_J multiplets is typical for Eu^{3+} β-diketones.[50,53] The differences in the splitting of the $^5D_0 \rightarrow {}^7F_2$ transition are because of distortions from the '*ideal*' tricapped-trigonal-prismatic coordination geometry of Eu^{3+} ions induced by the variations of the steric hindrance of the Al^{3+}-coordinated L ligands.

To evaluate the effects of the different Al(L)$_3$ moiety on luminescence properties, quantitative data such as absolute photoluminescence quantum yield and sensitization efficiency are needed (Table S2). In addition, comparison of experimental (τ_{exp}) and radiative lifetimes (τ_{rad}) provides insights into nonradiative deactivation processes, the latter being the longest emission lifetime for the $^5D_0$ excited state achievable in absence of nonradiative deactivation channels. These quantities are determined from the Eu^{3+} emission spectra following a well-established procedure.[51]

The data reported in Table S2 show a marked difference between the samples: **1Eu** and **2Eu** have PLQY $\geq$10%, whereas the emission of **3Eu** is strongly quenched. The same trend is observed for the experimental lifetimes.

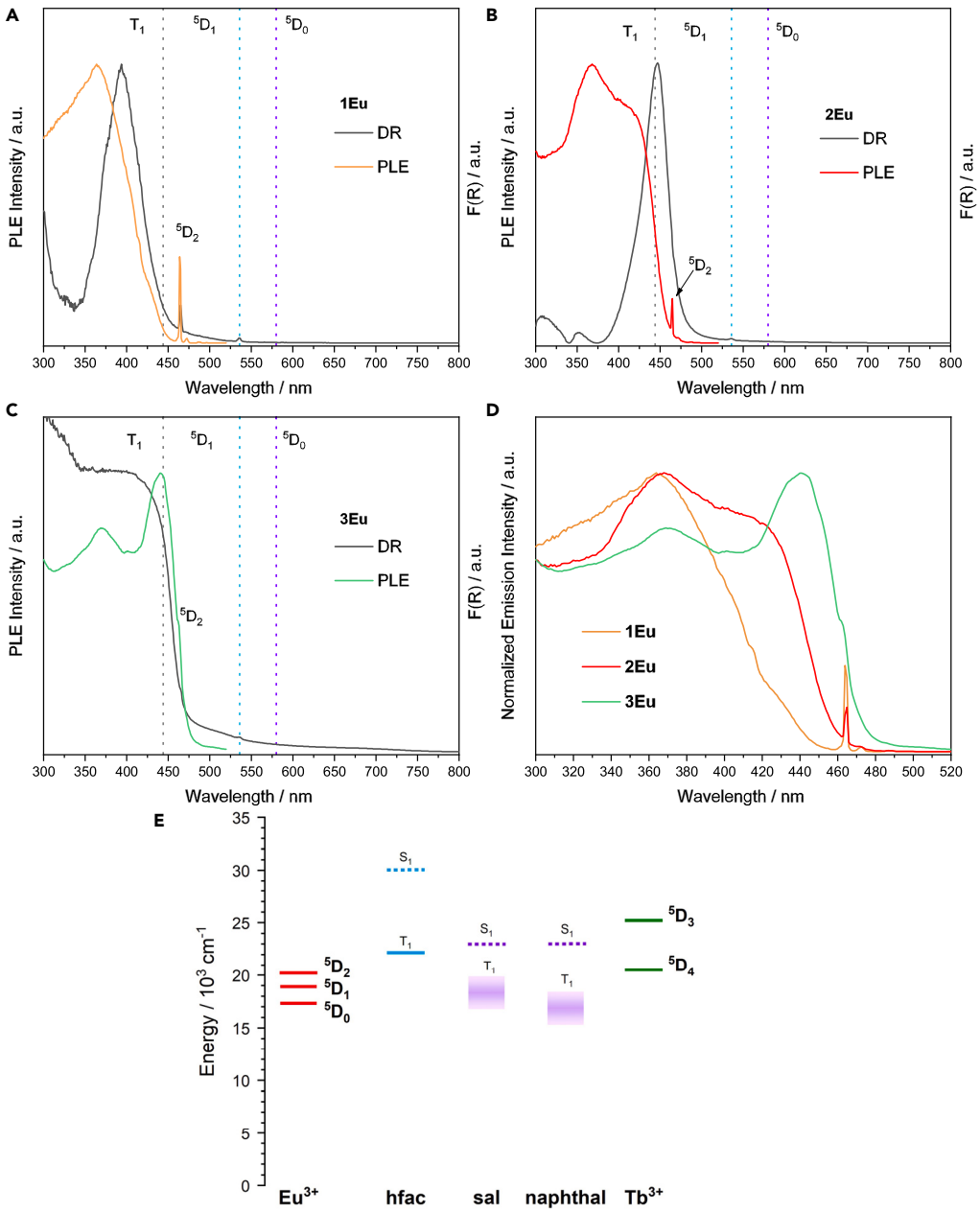

Figure 7. Overlap of diffuse reflectance (DR) and photoluminescence excitation spectra (PLE)

(A–D) Overlap of diffuse reflectance (DR) and photoluminescence excitation spectra (PLE) for A); B); C). D) Overlap of PLE spectra of **1Eu**, **2Eu**, and **3Eu**. The vertical dotted lines highlight the position of the hfac triplet level (T_1) determined from the emission spectra of **1Gd**, **2Gd,** and **3Gd** complexes (Figure S8) recorded at 77 K, and the first two Eu^{3+} excited states ($^5D_1$ and $^5D_0$).

(E) Simplified energy level diagram reporting the excited states of Eu^{3+}, Tb^{3+}, and L ligands involved in the sensitized emission process. S_1 and T_1 indicates excited singlet and triplet states respectively. Triplet levels of sal and naphthal are indicated as boxes to evidence the higher uncertainties on their energy because of the broadness of the spectra used for their determination (Figure S8). S_1 and T_1 for meac are not reported because they fall at $\lambda < 300$ nm ($E >$ ca. 33300 cm^{-1}), i.e., outside the investigated range.

For **1Eu** and **2Eu**, τ_{exp} are around 0.6 ms and become about one order of magnitude shorter in **3Eu**. Even the emissive complexes show significant differences: the highest photoluminescence quantum yield is observed for **2Eu** and is almost double that of **1Eu**. Same behavior is observed for the sensitization efficiency $\eta_{2Eu}/\eta_{1Eu} \approx 1.7$.

Discussing the absorption spectra, we pointed out that for all the complexes there are absorption tails extending toward the visible region that, in principle, could affect the emission properties because of interactions with europium excited states. In this regard, it is interesting to compare the photoluminescence excitation (PLE) and absorption spectra (Figure 7). The positions of the most relevant LC and MC states, *i.e.* T_1 for the Gd(hfac)$_3$ moiety, $^5D_1$, and $^5D_0$, are evidenced in the spectra by vertical dotted lines. The $^5D_2$ state is clearly visible in the PLE spectra of **1Eu** and **2Eu** at 464 nm but it appears only as a low intensity shoulder in the spectra of **3Eu**.

The emission behavior of the **1Eu**, **2Eu** and **3Eu** complexes can be elucidated by means of a simplified model consisting in two non-interacting excitation paths involving hfac or Al(L)$_3$ ligands respectively. To simplify the discussion, the two paths will be labeled Path-hfac and Path-L. So far, we considered (Figures 7A–D) only the triplet level of Eu(hfac)$_3$ fragment (T_1^{hfac} = 22100 cm^{-1}) but it is not enough to fully justify the experimental data. Concerning Al(L)$_3$ moieties, the energy of the first singlet excited state of L ligands decreases with the introduction of aromatic rings in the ligand structure; that is, methyl acetoacetate (**1Ln**) > salicylaldehyde (**2Ln**) ≥ 2-hydroxynaphthaldehyde (**3Ln**). The absorption onsets of their absorption spectra (Figures 5A–5C) are 315 nm for methyl acetoacetate and *ca.* 475 nm for both sal and naphthal. The energy of the first excited triplet state lowers (T_1^{sal} = 18400 cm^{-1}, T_1^{naf} = 17800 cm^{-1}) accordingly and become quite close, or even lower for **3Eu**, to those of the $^5D_1$ and $^5D_0$ Eu^{3+} excited states, Figures 7E and S8. In **1Eu** we find the simplest situation: Path-hfac and Path-L have quite different energies (Figures 5A and S8) and only the former is active. Noteworthy, Eu(hfac)$_3$ 2H$_2$O and **1Eu** displays the same value of PLQY (Table S2). In **2Eu**, the energy of the two channels becomes comparable and both can sensitize europium emission. Instead, only the absorption of the naphthal ligand is observed in the absorption spectrum of **3Eu** (Figure 5C), for which the predominant path is Path-L. The reduction of the energy gap between the L triplet (Figures 7E and S8) and $^5D_{0,1}$ causes the quenching of the Eu^{3+} emissions. In addition to ligand-centered transitions, also LMCTs can affect the emission properties of **1Eu**, **2Eu** and **3Eu.** As a general rule, the effect of the LMCT transitions strongly depends on their energy.[54–58] High energy LMCT, close to excited LC singlet and triplet states, can act as quenching channels because they could interfere with the energy transfer populating Eu^{3+} emissive states. Conversely, when they fall close to $^5D_1$ and $^5D_0$, they trigger the nonradiative deactivation of these MC excited states. These two examples represent limit cases, but intermediate situations with lower LMCT states quenching efficiency are possible.[54] For **1Eu** the maximum of CT band lies in between S_1 and T_1 and the observed values for a PLQY (10%) and sensitization efficiency (14.7%) indicate the presence of some quenching active throughout the LC channel. In **2Eu**, the aromaticity is introduced through the L ligand and the CT energy lowers deactivating the quenching path and boosting the Eu^{3+} emission. **2Eu** is the brighter emitter of the investigated complexes (Table S2). In **3Eu** the situation is more complicated because of the overlap between LC and LMCT transitions (Figure 5C) that does not allow to extract clear information. However, the observed emission properties can be well justified considering only the excitation path (Path-L) through Al(L)$_3$ moieties.

In addition to Eu^{3+}, Tb^{3+} is another lanthanide often used in combination with europium, equally interesting for its emission properties. Studying **nEu** and **nGd** complexes, we achieved good know-how of the photophysics of [Eu(hfac)$_3$Al(L)$_3$] complexes that we will use to extend the study to Tb^{3+} analogs. Concerning the electronic structure, terbium is more complex than europium and its first excited state $^5D_4$, with energy of ca. 20500 cm^{-1}, lies about 3000 cm^{-1} above the Eu^{3+} $^5D_0$.

From the comparison of absorption spectra of **1Gd** and **1Tb** (Figure 8A) we can infer that the observed bands are largely because of LCMT transitions in analogy of **1Eu**. Unlike europium, as soon as we introduce an aromatic ligand, the spectra of the heteronuclear complex (**2Tb**, Figure 8B) and of the Al(L)$_3$ moiety are almost superimposable. For **3Tb** (Figure 8C) the situation is equivalent indicating that for these complexes the absorption, largely because of the L and LMCT, if present, are shadowed by the LC related to the Al(L)$_3$ fragment.

The photoluminescence of the **nTb** complexes resulted strongly dependent from L. When excited at 370 nm all samples emitted light but only for **1Tb** a bright green emission (PLQY = 27%) from Tb^{3+} ions was detected. Conversely, in **2Tb** and **3Tb** the emissions have low intensity and the spectra have the typical shape of ligand-centered fluorescence attributed to Al(L)$_3$ moieties (Figure 8D). The tuning of excitation wavelength did not produce appreciable effects. In these complexes, the optically active portion of the complex is on Al(L)$_3$ ligands, as observed also in the absorption spectra. The model used for europium is valid also for Tb^{3+} complexes. In all but **1Tb** the dominant excitation path is Path-L in which the triplet energies are too low (Figure 7E) to allow an efficient energy transfer.

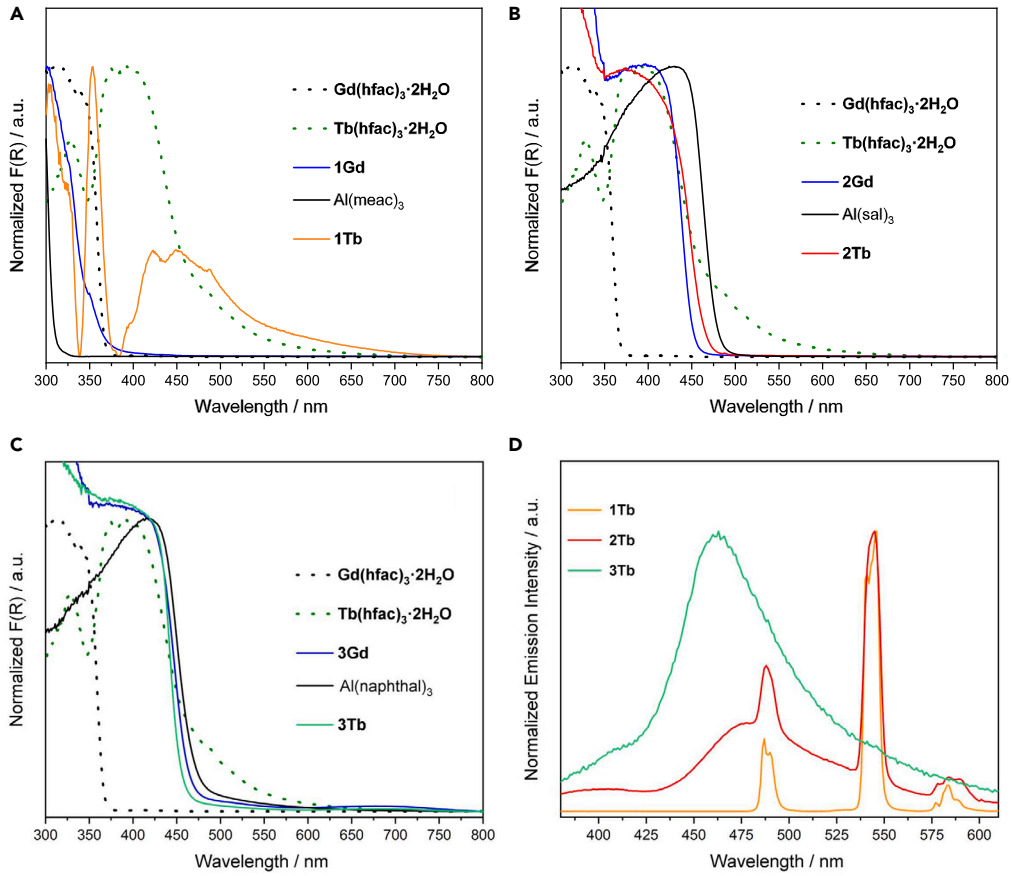

Figure 8. Diffuse reflectance spectra of samples powders of 1Tb, 2Tb, and 3Tb

(A–C) Diffuse reflectance spectra of samples powders of (A) **1Tb**, (B) **2Tb**, and (C) **3Tb**. The spectra of the corresponding $Al(L)_3$ and gadolinium complexes are added for comparison. (D) Emission spectra of **nTb** (**n** = **1**, **2**, and **3**).

Simulated absorption spectra

The hypothesis of electronic transitions localized on $Eu(hfac)_3$ and $Al(L)_3$ well explains the absorption/emission behavior for the different ligands, where different deactivation mechanisms for Ln^{3+} emissions can be invoked. In more detail, this means that even if one observes experimentally and computationally the formation of the $[Ln(hfac)_3Al(L)_3]$ heterometallic complexes, the initial and final electronic states involved in the light absorption are both located on the $Eu(hfac)_3$ or $Al(L)_3$ fragment. For the light absorption, only a weak interaction between the two moieties of the heterometallic complexes is supposed. Then, in addition to the spectroscopy outcomes, further support for this hypothesis can be gained by comparing the simulated absorption spectra for the $Eu(hfac)_3$ and $Al(L)_3$ complexes (see Figure S9) with the experimental ones for the $[Ln(hfac)_3Al(L)_3]$ heterometallic complexes. A detailed description of the comparison between experimental and simulated spectra for monometallic $Eu(hfac)_3$ and $Al(L)_3$ complexes is in the Supporting Information. The proper simulation of the absorption spectra for the monometallic complexes is crucial because a direct comparison between them and the experimental $[Eu(hfac)_3Al(L)_3]$ ones will allow us to study the interaction between the two parts (Eu and Al ones). The overlaps between the simulated spectra for the $Eu(hfac)_3$ and all $Al(L)_3$ complexes and the experimental **1Eu**, **2Eu** and **3Eu** in solution are reported in Figure 9. The **1Eu** spectrum shows two distinct peaks of similar intensity at 4 and 4.75 eV. Comparison with the simulated spectrum allows us to assign the higher energy peak to the $Al(meac)_3$ complex, and the lower energy one to $Eu(hfac)_3$ (Figure 9A).

The **2Eu** spectrum has multiple features: the higher peak is around 5.75 eV, while two less intense peaks are present around 4 and 4.75 eV. For this complex as well, the simulated spectrum assigns the two higher energy peaks to the $Al(sal)_3$ complex and the lower energy one again to $Eu(hfac)_3$ (Figure 9B). Finally, the **3Eu** spectrum has two main peaks with different intensities: the highest one at 5.6 eV and the lowest at around

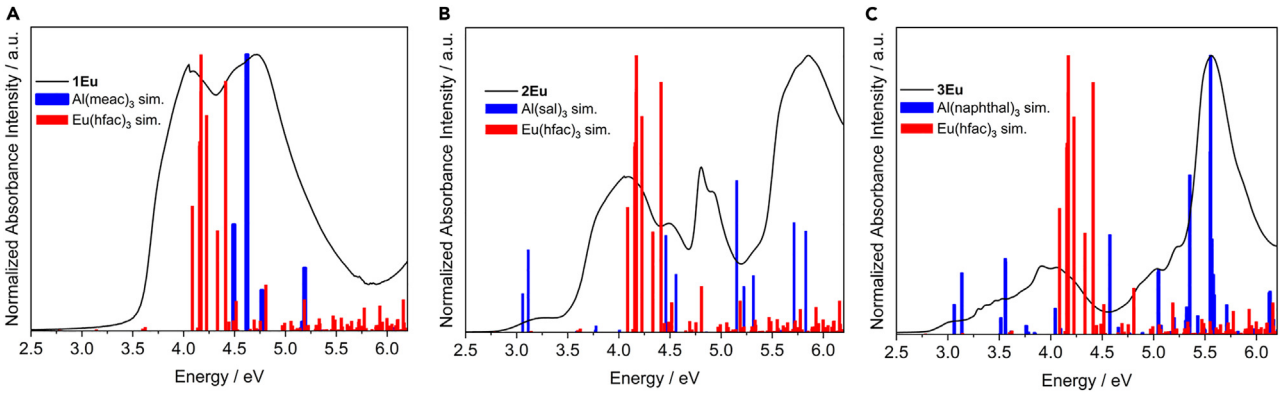

Figure 9. Comparison of simulated and experimental absorption spectra

(A–C) Normalized experimental (solid black lines) for **1Eu** (A), **2Eu** (B) and **3Eu** (C) and simulated electronic absorption spectra (blue bars) for $Al(meac)_3$(A), $Al(sal)_3$(B) and $Al(naphthal)_3$(C) and simulated electronic absorption spectra (red bars) for $Eu(hfac)_3$. A fixed shift of 0.80 eV is applied to all $Al(L)_3$ complexes spectra, whereas a shift of 0.66 eV is applied for $Eu(hfac)_3$ spectrum. Level of theory: CAM-B3LYP/TZ2P.

4 eV. In analogy with the two previous **1Eu** and **2Eu** complexes, the higher energy peak is because of the $Al(naphthal)_3$ complex, while the lower energy is because of $Eu(hfac)_3$ (Figure 9C). Common trends can be inferred from the analysis of the **1Eu**, **2Eu** and **3Eu** spectra: (1) The higher energy part (above 4.5 eV) of the heterometallic complex spectra is because of the $Al(L)_3$ complex; (2) the central part around 4.2 eV is mainly because of $Eu(hfac)_3$, and (3) the lower energy part (below 3.6 eV) is strongly sensitive to the Al complex.

Moreover, the comparison between the experimental and simulated spectra for all complexes shows that in the heterometallic complex spectra the maximum peak in the Eu part is slightly shifted at lower energies with respect to the monometallic europium complex, whereas no shifts are observed for the Al part (Figure 9). This behavior can be explained by considering the variations of the geometrical structure for the Eu and Al fragments switching from monometallic to heterometallic complexes. The root-mean-square distances (RMSDs) can quantify the difference between two structures. The comparison between the geometrical parameters of the Al fragment in $Al(L)_3$ complexes and in $[Eu(hfac)_3Al(L)_3]$ results in very small values (0.18, 0.10 and 0.52 for meac, sal, and naphthal ligands, respectively). The same comparison performed on the Eu fragment in $Eu(hfac)_3$ and in $[Eu(hfac)_3Al(L)_3]$ yields values of 4.96, 5.28 and 3.12 for the meac, sal, and naphthal ligands, respectively. These values mean that the Eu fragment undergoes a large structural rearrangement in the heterometallic complex formation, whereas the Al part is almost unchanged. This significant variation of the geometrical parameters, also highlighted in the discussion of the emission spectra (Figure 6), explains the shift to lower energies observed only for the Eu part in the heterometallic complex spectrum. All theoretical outcomes confirm that the absorption spectra of the heterometallic complexes can be roughly obtained as the sum of two contributions: one from the $Al(L)_3$ complex and one from the $Eu(hfac)_3$ fragment. There is no evidence in all $[Eu(hfac)_3Al(L)_3]$ spectra for the presence of new additional peaks attributable to a significant interaction between the two parts of the complexes. Moreover, no additional shifts must be applied to $Al(L)_3$ or $Eu(hfac)_3$ complexes to correctly fall into the features of the experimental $[Eu(hfac)_3Al(L)_3]$ spectra.

Additional information on the role of the different L ligands can be obtained from the lower energy range. Figure 10 shows that between 3.6 eV and 2.8 eV the contribution of the ligand varies: in **1Eu**, the observed band is only because of $Eu(hfac)_3$ whereas in **2Eu** and **3Eu** bearing aromatic L ligands new transitions are observed. Figure 10 reports the low energy region of the absorption spectra of **2Eu** and **3Eu**, together with a detailed analysis of the two most intense electronic transitions (labeled with arrows in Figure 10). The complete description of all electronic transitions involved in this portion of the spectrum is shown in the Supplementary Information Figures S11 and S12.

In more details, in **2Eu** the simulation assigns the peak around 3.1 eV to ligand-to-ligand electronic transition from HOMO to LUMO in the $Al(sal)_3$ complex (see Figure 10). Similarly, the experimental spectrum for **3Eu** shows a peak around 3.1 eV, also because of HOMO to LUMO transitions, and an additional feature around 3.5 eV because of HOMO-3 and HOMO-4 to LUMO transitions localized on the $Al(naphthal)_3$ complex. The analysis of the MOs of the two complexes point out strong similarities in the MOs involved in the

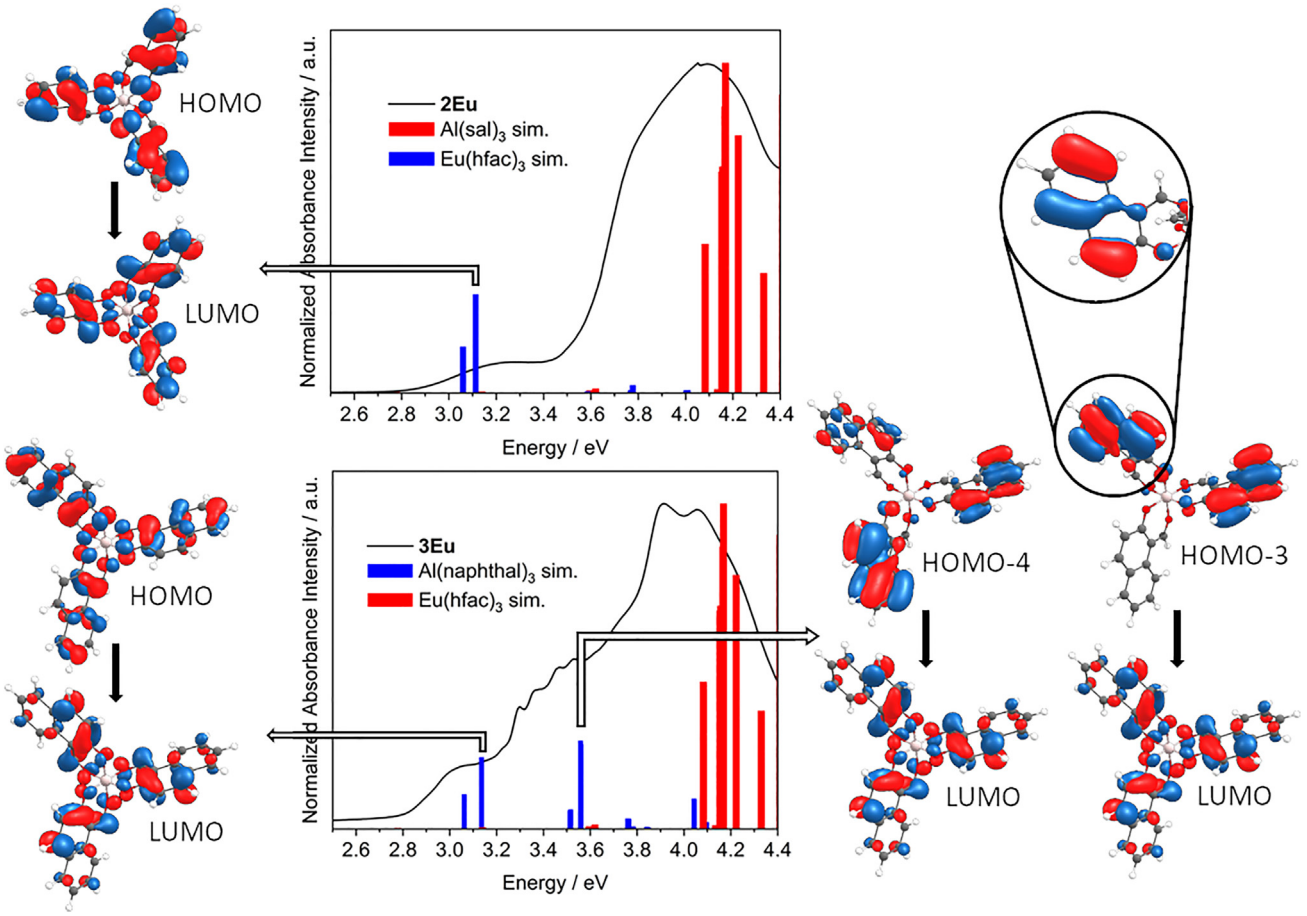

Figure 10. Comparison of simulated and experimental absorption spectra

Molecular Orbitals involved in the most intense Al complexes electronic transitions are included. Experimental spectra (solid lines) for **2Eu** and **3Eu** and simulated (bars) spectra for $Al(sal)_3$, $Al(naphthal)_3$, and $Eu(hfac)_3$ complexes (blue bars for Al complexes, red for the Eu one). A fixed shift of 0.80 eV is applied to all $Al(L)_3$ complexes spectra, whereas a shift of 0.66 eV is applied for $Eu(hfac)_3$ spectrum. The cut part of the experimental spectra is normalized to better appreciate the shape of this portion. MOs involved in the most intense Al complexes electronic transitions are included in the figure. The inset shows a rotated view of the aromatic ring of the naphthalene fragment involved in the higher energy electronic transition.

transition around 3.1 eV (see Figure 10, MOs in the left side), *i.e.*, electronic density is spread over the whole ligand both in the HOMO and in the LUMO. Conversely, the transition at 3.5 eV in the spectrum of **3Eu** originates from a HOMO totally localized on the external aromatic ring of naphthalene (see Figure 10, MOs in the right side and the inset) that is not present in the **2Eu** ligand.

Conclusions

In conclusion, we report the synthesis of a series of heterometallic Ln^{3+}-Al^{3+} (Ln^{3+} = Eu^{3+}, Gd^{3+}, and Tb^{3+}) complexes with composition $[Ln(hfac)_3Al(L)_3]$ (L = meac, sal, naphthal) in mild conditions and good yields. They have been obtained by reaction of the formally coordinatively unsaturated lanthanide fragment $[Ln(hfac)_3]$ with the corresponding octahedral $[Al(L)_3]$ complex. This general synthetic procedure, previously applied only for acac complexes for M^{3+} metal ions, can be used to prepare heterometallic complexes with many other mononuclear octahedral complexes with symmetric or asymmetric chelate oxygen donor ligands acting as Lewis basic sites. In this report we show that it is possible to modify the coordination sphere on the aluminum center still obtaining heterometallic dinuclear complexes where the europium center has a tricapped-trigonal-prismatic coordination geometry and shares a trigonal face with the aluminum octahedron. It is noteworthy that these acid to base interactions are stable also in solution in non-polar solvents. In these compounds, two different metals get quite close to each other (about 3.2 Å) in the same molecular architecture so that their individual properties could be influenced, and a combined effect different from

the sum of the two contributes could result in their reactivity and in their magnetic and spectroscopic properties. This route can be exploited in future studies to develop a library of heterometallic complexes.

In the family of $[Ln(hfac)_3Al(L)_3]$ considered in this study, **1Eu**, **2Eu** and **1Tb** showed the bright red and green emission typical for europium and terbium complexes, respectively. Conversely, the emissions of **3Eu**, **2Tb** and **3Tb** complexes are strongly quenched. We showed that this behavior is well described by means of a simplified model consisting in two non-interacting excitation paths involving hfac or $Al(L)_3$ ligands respectively. In **1Eu**, we find the simplest situation: the two paths have quite different energies and only the one through hfac ligands is operative. In **2Eu**, the energy of the two channels becomes comparable and both can sensitize europium emission. Finally, for **3Eu** the absorption spectrum is dominated by naphthal-centered transitions. In this case the triplet energy is too low to effectively sensitize europium emissions. The model used for europium is valid also for Tb^{3+} complexes, but because of the higher energy of Tb^{3+} excited states respect to those of Eu^{3+}, the emissions of all but **1Tb** complexes are quenched. DFT calculations further supported the hypothesis that the electronic transitions are localized on one fragment of the complexes ($Eu(hfac)_3$ and $Al(L)_3$). Then, for the absorption/emission behavior, only a weak interaction between the two fragments of the heterometallic complexes is found. In fact, the experimental absorption spectra of the heterometallic complexes are well simulated as the sum of the calculated spectra of the two monometallic complexes.

Limitation of the study

In the present work we developed a family of hetero-bimetallic complexes of general formula $[Ln(hfac)_3Al(L)_3]$ in which the ligands of $Al(L)_3$ fragments have increasing aromaticity. Instead, the steric and electronic effects on the ligands coordinated only to Ln^{3+} cations were not investigated. We will address this aspect in forthcoming studies. The comparison of emission properties other with Eu-Al or Tb-Al complexes is not possible because we did not find data in the literature. NMR characterization is precluded for terbium (giving for our samples unsatisfactory spectra) and for gadolinium (not suitable for NMR experiments).

STAR★METHODS

Detailed methods are provided in the online version of this paper and include the following:

- KEY RESOURCES TABLE
- RESOURCE AVAILABILITY
  - Lead contact
  - Materials availability
  - Data and code availability
- METHOD DETAILS
  - Computational details
  - Synthesis of $[Ln(hfac)_3Al(meac)_3]$ (Ln^{3+}= Eu^{3+}, Gd^{3+}, and Tb^{3+})
  - Synthesis of $[Ln(hfac)_3Al(sal)_3]$ (Ln^{3+}= Eu^{3+}, Gd^{3+}, and Tb^{3+})
  - Synthesis of $[Ln(hfac)_3Al(naphthal)_3]$ (Ln^{3+}= Eu^{3+}, Gd^{3+}, and Tb^{3+})

SUPPLEMENTAL INFORMATION

Supplemental information can be found online at https://doi.org/10.1016/j.isci.2023.106614.

ACKNOWLEDGMENTS

G.B. and L.A. thank the National Research Council PROGETTI@CNR P@CNR_01_ TerMoSmart and University of Padova P-DiSC#01-BIRD2021 for financial support. L.L. and S.S. acknowledge the financial support of Pisa University (Fondi di Ateneo 2023). This work is supported by the Università di Pisa under the "PRA – Progetti di Ricerca di Ateneo" (Institutional ResearchGrants) – Project no. PRA_2022_12 "New challenges of transition metal and lanthanide complexes in the perspective of green chemistry".

AUTHOR CONTRIBUTIONS

L.L., G.B., and S.C. conceived the project. L.B., E.G., L.L., and S.S. performed the synthesis and NMR characterization. F.M. performed structural characterization. G.B. performed the photophysical studies. S.C. and L.B. performed the DFT calculations. L.A. fueled constructive discussions on the experimental design

and data interpretation. L.L., G.B., and S.C. drafted the manuscript. All authors contributed to the analysis of the results and the writing of the manuscript.

DECLARATION OF INTERESTS

The authors declare no competing interests.

Received: January 26, 2023
Revised: March 15, 2023
Accepted: March 31, 2023
Published: April 11, 2023

REFERENCES

1. Pierre, V.C., Botta, M., Aime, S., and Raymond, K.N. (2006). Fe(III)-Templated Gd(III) self-AssembliesA new route toward macromolecular MRI contrast agents. J. Am. Chem. Soc. *128*, 9272–9273. https://doi.org/10.1021/ja061323j.

2. Crowston, B.J., Shipp, J.D., Chekulaev, D., McKenzie, L.K., Jones, C., Weinstein, J.A., Meijer, A.J.H., Bryant, H.E., Natrajan, L., Woodward, A., and Ward, M.D. (2019). Heteronuclear d–d and d–f Ru(II)/M complexes [M = Gd(III), Yb(III), Nd(III), Zn(II) or Mn(II)] of ligands combining phenanthroline and aminocarboxylate binding sites: combined relaxivity, cell imaging and photophysical studies. Dalton Trans. *48*, 6132–6152. https://doi.org/10.1039/C9DT00954J.

3. Li, H., Lan, R., Chan, C.-F., Jiang, L., Dai, L., Kwong, D.W.J., Lam, M.H.-W., and Wong, K.-L. (2015). Real-time in situ monitoring via europium emission of the photo-release of antitumor cisplatin from a Eu–Pt complex. Chem. Commun. *51*, 14022–14025. https://doi.org/10.1039/C5CC05461C.

4. Al-Busaidi, I.J., Ilmi, R., Dutra, J.D.L., Oliveira, W.F., Haque, A., Al Rasbi, N.K., Marken, F., Raithby, P.R., and Khan, M.S. (2021). Utilization of a Pt(II) di-yne chromophore incorporating a 2,2′-bipyridine-5,5′-diyl spacer as a chelate to synthesize a green and red emitting d–f–d heterotrinuclear complex. Dalton Trans. *50*, 1465–1477. https://doi.org/10.1039/D0DT04198J.

5. Tropiano, M., Kilah, N.L., Morten, M., Rahman, H., Davis, J.J., Beer, P.D., and Faulkner, S. (2011). Reversible luminescence switching of a redox-active ferrocene–europium dyad. J. Am. Chem. Soc. *133*, 11847–11849. https://doi.org/10.1021/ja203069s.

6. Shiga, T., Ohba, M., and Ōkawa, H. (2004). A series of trinuclear $Cu^{III}Ln^{III}Cu^{II}$ complexes derived from 2,6-Di(acetoacetyl)pyridine: synthesis, structure, and magnetism. Inorg. Chem. *43*, 4435–4446. https://doi.org/10.1021/ic034998l.

7. Yamaguchi, T., Sunatsuki, Y., Ishida, H., Kojima, M., Akashi, H., Re, N., Matsumoto, N., Pochaba, A., and Mroziński, J. (2008). Synthesis, structures, and magnetic properties of face-sharing heterodinuclear Ni(II)−Ln(III) (Ln = Eu, Gd, Tb, Dy) complexes. Inorg. Chem. *47*, 5736–5745. https://doi.org/10.1021/ic8000575.

8. Shen, F.-X., Li, H.-Q., Miao, H., Shao, D., Wei, X.-Q., Shi, L., Zhang, Y.-Q., and Wang, X.-Y. (2018). Heterometallic $M^{II}Ln^{III}$ (M = Co/Zn; Ln = Dy/Y) complexes with pentagonal bipyramidal 3d centers: syntheses, structures, and magnetic properties. Inorg. Chem. *57*, 15526–15536. https://doi.org/10.1021/acs.inorgchem.8b02875.

9. Yang, Q.-Y., Li, K., Luo, J., Pan, M., and Su, C.-Y. (2011). A simple topological identification method for highly (3,12)-connected 3D MOFs showing anion exchange and luminescent properties. Chem. Commun. *47*, 4234–4236. https://doi.org/10.1039/C0CC05464J.

10. Beer, P.D., Szemes, F., Passaniti, P., and Maestri, M. (2004). Luminescent ruthenium(II) Bipyridine−Calix[4]arene complexes as receptors for lanthanide cations. Inorg. Chem. *43*, 3965–3975. https://doi.org/10.1021/ic0499401.

11. Zhu, Q.-Y., Zhou, L.-P., and Sun, Q.-F. (2019). Strongly luminescent 5d/4f heterometal–organic macrocycles with open metal sites: post-assembly modification and sensing. Dalton Trans. *48*, 4479–4483. https://doi.org/10.1039/C9DT00710E.

12. Ziessel, R., Diring, S., Kadjane, P., Charbonnière, L., Retailleau, P., and Philouze, C. (2007). Highly efficient blue photoexcitation of europium in a bimetallic Pt–Eu complex. Chem. Asian J. *2*, 975–982. https://doi.org/10.1002/asia.200700143.

13. Mori, F., Nyui, T., Ishida, T., Nogami, T., Choi, K.-Y., and Nojiri, H. (2006). Oximate-bridged trinuclear Dy−Cu−Dy complex behaving as a single-molecule magnet and its mechanistic investigation. J. Am. Chem. Soc. *128*, 1440–1441. https://doi.org/10.1021/ja057183f.

14. Armelao, L., Dell'Amico, D.B., Bottaro, G., Bellucci, L., Labella, L., Marchetti, F., Mattei, C.A., Mian, F., Pineider, F., Poneti, G., and Samaritani, S. (2018). 1D hetero-bimetallic regularly alternated 4f–3d coordination polymers based on N-oxide-4,4′-bipyridine (bipyMO) as a linker: photoluminescence and magnetic properties. Dalton Trans. *47*, 8337–8345. https://doi.org/10.1039/C8DT00880A.

15. Costes, J.-P., Dahan, F., Dupuis, A., and Laurent, J.-P. (1997). A general route to strictly dinuclear Cu(II)/Ln(III) complexes. Structural determination and magnetic behavior of two Cu(II)/Gd(III) complexes. Inorg. Chem. *36*, 3429–3433. https://doi.org/10.1021/ic970264v.

16. Gao, T., Yan, P.-F., Li, G.-M., Hou, G.-F., and Gao, J.-S. (2008). N,N′-Ethylene-bis(3-methoxysalicylideneimine) mononuclear (4f) and heterodinuclear (3d–4f) metal complexes: synthesis, crystal structure and luminescent properties. Inorg. Chim. Acta. *361*, 2051–2058. https://doi.org/10.1016/j.ica.2007.10.021.

17. Visinescu, D., Alexandru, M.-G., Madalan, A.M., Pichon, C., Duhayon, C., Sutter, J.-P., and Andruh, M. (2015). Magneto-structural variety of new 3d–4f–4(5)d heterotrimetallic complexes. Dalton Trans. *44*, 16713–16727. https://doi.org/10.1039/C5DT01738F.

18. Øwre, A., Vinum, M., Kern, M., Van Slageren, J., Bendix, J., and Perfetti, M. (2018). Chiral, heterometallic lanthanide–transition metal complexes by design. INORGA *6*, 72. https://doi.org/10.3390/inorganics6030072.

19. Lindoy, L.F., Lip, H.C., Louie, H.W., Drew, M.G.B., and Hudson, M.J. (1977). Interaction of lanthanide shift reagents with co-ordination complexes; direct observation of nuclear magnetic resonance signals for free and complexed tris(pentane-2,4-dionato) cobalt(III) at ambient temperature, and X-ray crystal and molecular structure of the 1 : 1 adduct formed. J. Chem. Soc., Chem. Commun. 778–780. https://doi.org/10.1039/C39770000778.

20. Ramade, I., Kahn, O., Jeannin, Y., and Robert, F. (1997). Design and Magnetic Properties of a Magnetically Isolated GdIIICuII Pair. Crystal Structures of $[Gd(hfa)_3Cu(salen)]$, $[Y(hfa)_3Cu(salen)]$, $[Gd(hfa)_3Cu(salen)(Meim)]$, and $[La(hfa)_3(H_2O)Cu(salen)]$ [hfa = Hexafluoroacetylacetonato, salen = N,N′-Ethylenebis(salicylideneaminato), Meim = 1-Methylimidazole]. Inorg. Chem. *36*, 930–936. https://doi.org/10.1021/ic9607595.

21. Rogachev, A.Y., Mironov, A.V., and Nemukhin, A.V. (2007). Experimental and theoretical studies of the products of reaction between $Ln(hfa)_3$ and $Cu(acac)_2$ (Ln=La, Y; acac=acetylacetonate, hfa=hexafluoroacetylacetonate). J. Mol. Struct. *831*, 46–54. https://doi.org/10.1016/j.molstruc.2006.07.018.

22. Kameta, N., Imura, H., Ohashi, K., and Aoyama, T. (1999). Equilibrium and spectroscopic studies on the complexation of tris(1-(2-thienyl)-4,4,4-trifluoro-1,3-butanedionato)lanthanoids(III) with tris(2,4-pentanedionato)cobalt(III) as complex ligand. Inorg. Chem. Commun. *2*, 124–127. https://doi.org/10.1016/S1387-7003(99)00027-1.

23. Kameta, N., Imura, H., Ohashi, K., and Aoyama, T. (2002). Stability constants of inner- and outer-sphere complexes of hydrated tris(1-(2-thienyl)-4,4,4-trifluoro-1,3-butanedionato) lanthanide(III) with tris(2,4-pentanedionato) cobalt(III). Polyhedron *21*, 805–810. https://doi.org/10.1016/S0277-5387(02)00858-6.

24. Lieberman, C.M., Wei, Z., Filatov, A.S., and Dikarev, E.V. (2016). Mixed-ligand approach to changing the metal ratio in bismuth–transition metal heterometallic precursors. Inorg. Chem. *55*, 3946–3951. https://doi.org/10.1021/acs.inorgchem.6b00209.

25. Bellucci, L., Fioravanti, L., Armelao, L., Bottaro, G., Marchetti, F., Pineider, F., Poneti, G., Samaritani, S., and Labella, L. (2023). Size selectivity in heterolanthanide molecular complexes with a ditopic ligand. Chem. – eur. J. *29*, e202202823. https://doi.org/10.1002/chem.202202823.

26. Fioravanti, L., Bellucci, L., Armelao, L., Bottaro, G., Marchetti, F., Pineider, F., Poneti, G., Samaritani, S., and Labella, L. (2022). Stoichiometrically controlled assembly of lanthanide molecular complexes of the heteroditopic divergent ligand 4′-(4-Pyridyl)-2,2′:6′,2″-terpyridine N-oxide in hypodentate or bridging coordination modes. Structural, magnetic, and photoluminescence studies. Inorg. Chem. *61*, 265–278. https://doi.org/10.1021/acs.inorgchem.1c02809.

27. Bellucci, L., Bottaro, G., Labella, L., Marchetti, F., Samaritani, S., Belli Dell'Amico, D., and Armelao, L. (2021). 1D-Zigzag Eu^{3+}/Tb^{3+} coordination chains as luminescent ratiometric thermometers endowed with multicolor emission. Materials *14*, 6445. https://doi.org/10.3390/ma14216445.

28. Armelao, L., Dell'Amico, D.B., Bellucci, L., Bottaro, G., Di Bari, L., Labella, L., Marchetti, F., Samaritani, S., and Zinna, F. (2017). Circularly polarized luminescence of silica-grafted europium chiral derivatives prepared through a sequential functionalization. Inorg. Chem. *56*, 7010–7018. https://doi.org/10.1021/acs.inorgchem.7b00611.

29. Armelao, L., Belli Dell'Amico, D., Bellucci, L., Bottaro, G., Labella, L., Marchetti, F., and Samaritani, S. (2016). Smart grafting of lanthanides onto silica via N,N-dialkylcarbamato complexes. Inorg. Chem. *55*, 939–947. https://doi.org/10.1021/acs.inorgchem.5b02535.

30. Armelao, L., Belli Dell'Amico, D., Bellucci, L., Bottaro, G., Labella, L., Marchetti, F., and Samaritani, S. (2016). A convenient synthesis of highly luminescent lanthanide 1D-zigzag coordination chains based only on 4,4′-bipyridine as connector. Polyhedron *119*, 371–376. https://doi.org/10.1016/j.poly.2016.09.009.

31. Babetto, L., Carlotto, S., Carlotto, A., Rancan, M., Bottaro, G., Armelao, L., and Casarin, M. (2021). Multireference ab initio investigation on ground and low-lying excited states: systematic evaluation of J–J mixing in a Eu^{3+} luminescent complex. Inorg. Chem. *60*, 315–324. https://doi.org/10.1021/acs.inorgchem.0c02956.

32. Carlotto, A., Babetto, L., Carlotto, S., Miozzi, M., Seraglia, R., Casarin, M., Bottaro, G., Rancan, M., and Armelao, L. (2020). Luminescent thermometers: from a library of europium(III) β-diketonates to a general model for predicting the thermometric behaviour of europium-based coordination systems. ChemPhotoChem *4*. cptc.202000116. https://doi.org/10.1002/cptc.202000116.

33. Babetto, L., Carlotto, S., Carlotto, A., Rancan, M., Bottaro, G., Armelao, L., and Casarin, M. (2020). Antenna triplet DFT calculations to drive the design of luminescent Ln^{3+} complexes. Dalton Trans. *49*, 14556–14563. https://doi.org/10.1039/D0DT02624G.

34. Sanwaria, A.R., Nagar, M., Bohra, R., Chaudhary, A., Mobin, S.M., Mathur, P., and Choudhary, B.L. (2014). Sol–gel synthesis of highly pure α-Al_2O_3 nano-rods from a new class of precursors of salicylaldehyde-modified aluminum(III) isopropoxide. Crystal and molecular structure of $[Al(OC_6H_4CHO)_3]$. RSC Adv. *4*, 30081–30089. https://doi.org/10.1039/C4RA03245D.

35. Lichtenberger, R., Puchberger, M., Baumann, S.O., and Schubert, U. (2009). Modification of aluminum alkoxides with β-ketoesters: new insights into formation, structure and stability. J. Sol. Gel Sci. Technol. *50*, 130–140. https://doi.org/10.1007/s10971-008-1890-1.

36. Li, H., Zhang, F., Wang, Y., and Zheng, D. (2003). Synthesis and characterization of tris-(8-hydroxyquinoline)aluminum. Mater. Sci. Eng. B *100*, 40–46. https://doi.org/10.1016/S0921-5107(03)00067-9.

37. Lincoln, S. (2005). Mechanistic studies of metal aqua ions: a semi-historical perspective. Helv. Chim. Acta *88*, 523–545. https://doi.org/10.1002/hlca.200590036.

38. Yamamoto, M., Nakanishi, T., Kitagawa, Y., Seki, T., Ito, H., Fushimi, K., and Hasegawa, Y. (2018). Synthesis and photophysical properties of Eu(III) complexes with phosphine oxide ligands including metal ions. Bull. Chem. Soc. Jpn. *91*, 6–11. https://doi.org/10.1246/bcsj.20170241.

39. Xu, H.-B., Chen, X.-M., Zhang, Q.-S., Zhang, L.-Y., and Chen, Z.-N. (2009). Fluoride-enhanced lanthanide luminescence and white-light emitting in multifunctional Al_3Ln_2 (Ln = Nd, Eu, Yb) heteropentanuclear complexes. Chem. Commun. 7318–7320. https://doi.org/10.1039/B912474H.

40. Wang, S.-T., Zhang, S.-H., Fang, W.-H., and Zhang, J. (2020). Stepwise coordination assembly approach toward aluminum-lanthanide-based compounds. Inorg. Chem. *59*, 13760–13766. https://doi.org/10.1021/acs.inorgchem.0c02119.

41. Kühne, I.A., Griffiths, K., Hutchings, A.-J., Townrow, O.P.E., Eichhöfer, A., Anson, C.E., Kostakis, G.E., and Powell, A.K. (2017). Stepwise investigation of the influences of steric groups versus counterions to target Cu/Dy complexes. Cryst. Growth Des. *17*, 5178–5190. https://doi.org/10.1021/acs.cgd.7b00648.

42. Zhang, J., Li, C., Wang, J., Zhu, M., and Li, L. (2016). Slow magnetic relaxation behavior in rare Ln–Cu–Ln linear trinuclear complexes. Eur. J. Inorg. Chem. *2016*, 1383–1388. https://doi.org/10.1002/ejic.201501388.

43. Li, X.-L., Min, F.-Y., Wang, C., Lin, S.-Y., Liu, Z., and Tang, J. (2015). $[Ln^{III}–Mn^{II}–Ln^{III}]$ heterometallic compounds: rare linear SMMs with divalent manganese ions. Dalton Trans. *44*, 3430–3438. https://doi.org/10.1039/C4DT03713H.

44. Li, X.-L., Min, F.-Y., Wang, C., Lin, S.-Y., Liu, Z., and Tang, J. (2015). Utilizing 3d–4f magnetic interaction to slow the magnetic relaxation of heterometallic complexes. Inorg. Chem. *54*, 4337–4344. https://doi.org/10.1021/acs.inorgchem.5b00019.

45. Liu, S.-L., Wen, C.-L., Qi, S.-S., and Liang, E.-X. (2008). Synthesis and photoluminescence properties of novel europium complexes of 2′-hydroxyacetophenone and 4,6-diacetylresorcinol. Spectrochim. Acta Mol. Biomol. Spectrosc. *69*, 664–669. https://doi.org/10.1016/j.saa.2007.05.019.

46. Manseki, K., Hasegawa, Y., Wada, Y., and Yanagida, S. (2005). Photosensitized luminescence of thermostable polynuclear Eu(III) complexes. J. Lumin. *111*, 183–189. https://doi.org/10.1016/j.jlumin.2004.08.043.

47. Xu, C. (2006). Luminescent and thermal properties of Sm^{3+} complex with salicylate and o-phenanthroline incorporated in silica matrix. J. Rare Earths *24*, 429–433. https://doi.org/10.1016/S1002-0721(06)60137-3.

48. Xu, C.j., Yang, H., Xie, F., and Guo, X.z. (2005). Photoluminescence enhancement of Sm^{3+} in the Sm^{3+}–salicylic acid–o-phenanthroline ternary composite. J. Alloys Compd. *392*, 96–99. https://doi.org/10.1016/j.jallcom.2004.09.031.

49. De Bellis, J., Bellucci, L., Bottaro, G., Labella, L., Marchetti, F., Samaritani, S., Dell'Amico, D.B., and Armelao, L. (2020). Single-crystal-to-single-crystal post-synthetic modifications of three-dimensional LOFs (Ln = Gd, Eu): a way to modulate their luminescence and thermometric properties. Dalton Trans. *49*, 6030–6042. https://doi.org/10.1039/D0DT00449A.

50. Bellucci, L., Bottaro, G., Labella, L., Causin, V., Marchetti, F., Samaritani, S., Dell'Amico, D.B., and Armelao, L. (2020). Composition–Thermometric properties correlations in homodinuclear Eu^{3+} luminescent complexes. Inorg. Chem. *59*, 18156–18167. https://doi.org/10.1021/acs.inorgchem.0c02611.

51. Binnemans, K. (2015). Interpretation of europium(III) spectra. Coord. Chem. Rev. *295*, 1–45. https://doi.org/10.1016/j.ccr.2015.02.015.

52. Bellucci, L., Bottaro, G., Labella, L., Marchetti, F., Samaritani, S., Belli Dell'Amico, D., and Armelao, L. (2019). Luminescent sequence-dependent materials through a step by step assembly of RE^1–1,4-benzendicarboxylate–RE^2(RE^x = Y^{3+}, Eu^{3+} and Tb^{3+}) architectures on a silica surface. J. Mater. Chem. C *7*, 4415–4423. https://doi.org/10.1039/C9TC00181F.

53. Armelao, L., Belli Dell'Amico, D., Bellucci, L., Bottaro, G., Ciattini, S., Labella, L., Manfroni, G., Marchetti, F., Mattei, C.A., and Samaritani, S. (2018). Homodinuclear lanthanide complexes with the divergent heterotopic 4,4′-bipyridine N-oxide (bipyMO) ligand. Eur. J. Inorg. Chem. *2018*, 4421–4428. https://doi.org/10.1002/ejic.201800747.

54. Faustino, W.M., Malta, O.L., and de Sá, G.F. (2005). Intramolecular energy transfer through charge transfer state in lanthanide compounds: a theoretical approach. J. Chem. Phys. *122*, 054109. https://doi.org/10.1063/1.1830452.

55. Yanagisawa, K., Kitagawa, Y., Nakanishi, T., Seki, T., Fushimi, K., Ito, H., and Hasegawa, Y. (2018). A luminescent dinuclear Eu^{III}/Tb^{III} complex with LMCT band as a single-molecular thermosensor. Chem. Eur J. *24*, 1956–1961. https://doi.org/10.1002/chem.201705021.

56. Yanagisawa, K., Kitagawa, Y., Nakanishi, T., Akama, T., Kobayashi, M., Seki, T., Fushimi, K., Ito, H., Taketsugu, T., and Hasegawa, Y. (2017). Enhanced luminescence of asymmetrical seven-coordinate Eu^{III} complexes including LMCT perturbation. Eur. J. Inorg. Chem. *2017*, 3843–3848. https://doi.org/10.1002/ejic.201700815.

57. Ferreira da Rosa, P.P., Miyazaki, S., Sakamoto, H., Kitagawa, Y., Miyata, K., Akama, T., Kobayashi, M., Fushimi, K., Onda, K., Taketsugu, T., and Hasegawa, Y. (2021). Coordination geometrical effect on ligand-to-metal charge transfer-dependent energy transfer processes of luminescent Eu(III) complexes. J. Phys. Chem. A *125*, 209–217. https://doi.org/10.1021/acs.jpca.0c09337.

58. Kitagawa, Y., Ferreira da Rosa, P.P., and Hasegawa, Y. (2021). Charge-transfer excited states of π- and 4f-orbitals for development of luminescent Eu(III) complexes. Dalton Trans. *50*, 14978–14984. https://doi.org/10.1039/D1DT03019A.

59. Neese, F. (2018). Software update: the ORCA program system, version 4.0. WIREs Comput. Mol. Sci. *8*, e1327. https://doi.org/10.1002/wcms.1327.

60. Weigend, F., and Ahlrichs, R. (2005). Balanced basis sets of split valence, triple zeta valence and quadruple zeta valence quality for H to Rn: design and assessment of accuracy. Phys. Chem. Chem. Phys. *7*, 3297–3305. https://doi.org/10.1039/B508541A.

61. Weigend, F. (2008). Hartree–Fock exchange fitting basis sets for H to Rn. J. Comput. Chem. *29*, 167–175. https://doi.org/10.1002/jcc.20702.

62. Perdew, J.P., Burke, K., and Ernzerhof, M. (1996). Generalized gradient approximation made simple. Phys. Rev. Lett. *77*, 3865–3868. https://doi.org/10.1103/PhysRevLett.77.3865.

63. Perdew, J.P., and Wang, Y. (1992). Accurate and simple analytic representation of the electron-gas correlation energy. Phys. Rev. B *45*, 13244–13249. https://doi.org/10.1103/PhysRevB.45.13244.

64. Grimme, S., Antony, J., Ehrlich, S., and Krieg, H. (2010). A consistent and accurate ab initio parametrization of density functional dispersion correction (DFT-D) for the 94 elements H-Pu. J. Chem. Phys. *132*, 154104. https://doi.org/10.1063/1.3382344.

65. Parr, R.G., and Yang, W. (1984). Density functional approach to the frontier-electron theory of chemical reactivity. J. Am. Chem. Soc. *106*, 4049–4050. https://doi.org/10.1021/ja00326a036.

66. Perdew, J.P., Parr, R.G., Levy, M., and Balduz, J.L. (1982). Density-functional theory for fractional particle number: derivative discontinuities of the energy. Phys. Rev. Lett. *49*, 1691–1694. https://doi.org/10.1103/PhysRevLett.49.1691.

67. Yang, W., and Mortier, W.J. (1986). The use of global and local molecular parameters for the analysis of the gas-phase basicity of amines. J. Am. Chem. Soc. *108*, 5708–5711. https://doi.org/10.1021/ja00279a008.

68. Yanai, T., Tew, D.P., and Handy, N.C. (2004). A new hybrid exchange–correlation functional using the Coulomb-attenuating method (CAM-B3LYP). Chem. Phys. Lett. *393*, 51–57. https://doi.org/10.1016/j.cplett.2004.06.011.

69. Iikura, H., Tsuneda, T., Yanai, T., and Hirao, K. (2001). A long-range correction scheme for generalized-gradient-approximation exchange functionals. J. Chem. Phys. *115*, 3540–3544. https://doi.org/10.1063/1.1383587.

70. Jacquemin, D., Perpète, E.A., Scuseria, G.E., Ciofini, I., and Adamo, C. (2008). TD-DFT performance for the visible absorption spectra of organic dyes: conventional versus long-range hybrids. J. Chem. Theor. Comput. *4*, 123–135. https://doi.org/10.1021/ct700187z.

71. Zara, Z., Iqbal, J., Ayub, K., Irfan, M., Mahmood, A., Khera, R.A., and Eliasson, B. (2017). A comparative study of DFT calculated and experimental UV/Visible spectra for thirty carboline and carbazole based compounds. J. Mol. Struct. *1149*, 282–298. https://doi.org/10.1016/j.molstruc.2017.07.093.

72. Sheldrick, G.M. (2008). A short history of SHELX. Acta Crystallogr. A *64*, 112–122. https://doi.org/10.1107/S0108767307043930.

73. van der Sluis, P., and Spek, A.L. (1990). BYPASS: an effective method for the refinement of crystal structures containing disordered solvent regions. Acta Crystallogr. A *46*, 194–201. https://doi.org/10.1107/S0108767389011189.

STAR★METHODS

KEY RESOURCES TABLE

REAGENT or RESOURCE	SOURCE	IDENTIFIER
Chemicals, peptides, and recombinant proteins		
Europium oxide	Strem Chemicals	MFCD00010997
Terbium oxide	Strem Chemicals	MFCD00083151
Methyl acetoacetate	Merck Chemicals	537365
Aluminum isopropoxide	Merck Chemicals	220418
Salicylaldehyde	Merck Chemicals	S356
2-Hydroxy-1-naphthaldehyde	Merck Chemicals	H45353

RESOURCE AVAILABILITY

Lead contact

Further information and requests for resources should be directed to and will be fulfilled by the lead contact, Gregorio Bottaro (gregorio.bottaro@cnr.it).

Materials availability

Commercially available reagents were used without further purification.

All manipulations were performed under a dinitrogen atmosphere using anhydrous solvents.[Al(meac)$_3$] and [Al(sal)$_3$] were synthesized according to the literature.[34,35] [Al(naphthal)$_3$] was synthesized in a similar way. Anhydrous [Ln(hfac)$_3$] species (Ln^{3+} = Eu^{3+}, Gd^{3+} and Tb^{3+}) were obtained by dehydration of the corresponding dihydrate complex [Ln(hfac)$_3$(H$_2$O)$_2$] according to the procedure reported in the literature.[27] FTIR spectra on solid samples were recorded with a Perkin–Elmer ''Spectrum One'' spectrometer, equipped with an ATR accessory. ^{1}H and ^{19}F NMR spectra were recorded with a Bruker "Avance DRX400" spectrometer. Chemical shifts were measured in ppm (δ) from TMS by residual solvent peaks for ^{1}H, from CFCl$_3$ for ^{19}F. Elemental analysis (C, H, N) were performed with an Elementar "vario MICRO cube" instrument at Dipartimento di Chimica e Chimica Industriale, Università di Pisa. Absorption spectra were recorded using a Cary 5000 UV-Vis Spectrometer equipped with a diffuse reflectance accessory consisting of an integrating sphere. The spectra were acquired and plotted as the Kubelka–Munk function F(R). Luminescence spectra of sample powders were recorded with a Horiba JobinYvon *Fluorolog-3* spectrofluorimeter in a front-face acquisition geometry. The instrument was equipped with a double-grating monochromator in both the excitation and emission sides coupled to a *R928P* Hamamatsu photomultiplier and a 450 W Xe arc lamp as the excitation source. Emission spectra were corrected for detection and optical spectral response of the spectrofluorimeter supplied by the manufacturer. The excitation spectra were corrected for the spectral distribution of the lamp intensity using a photodiode reference detector. The luminescence lifetimes (τ_{exp}) were measured with an experimental uncertainty of $\pm$10%, using a pulsed Xe lamp with variable repetition rate and elaborated with standard software fitting procedures. Absolute photoluminescence quantum yields (PLQY) on samples powders were calculated from corrected emission spectra obtained by means of an integrating sphere. Estimated error on PLQY is $\pm$20%. The energy of triplet states of hfac and L ligands were estimated by taking the first maximum of the low temperature (77K) emission spectra of **1Gd**, **2Gd** and **3Gd**. The used bands are arrowed in Figure S8.

Data and code availability

Deposited data

X-ray crystallographic data CIF format (CCDC 2233057–2233060) can be obtained free of charge from the Cambridge Crystallographic Data Center, 12 Union Road, Cambridge CB2 1EZ, UK; fax: +44 1223 336 033; or e-mail: deposit@ccdc.cam.ac.uk.

METHOD DETAILS

Computational details

Calculations were carried out by using the Orca program (version 4.2.1).[59] Both DFT and wavefunction calculations were done using the all-electron triple-ζ quality Alrichs basis set with one polarization function (def2-TZVP)[60] for all atoms. Coulomb and exchange integrals were approximated by using the Resolution of Identity approximation with the def2/JK auxiliary basis set.[61] All geometry optimizations were carried out in gas phase using the PBE exchange-correlation functional[62,63] with the TightOpt setting. Frequency analyses were performed after each geometry optimization to ensure the absence of imaginary frequencies, confirming a minimum in the potential energy surface. Dispersion corrections were included in geometry optimizations by adopting Grimme's DFT-D3 method.[64]

The nucleophilicity of the two oxygen atoms in each ligand is calculated by using the Fukui function $f(r)$. It reflects the reactivity of a site and was defined by Parr and Yang[65] as the functional derivative of the chemical potential μ with respect to a change in the external potential $v(r)$, taken at a constant number of electrons N:

$$f(r) = \left[\frac{\delta\mu}{\delta v(r)}\right]_N \quad \text{(Equation 1)}$$

Due to a discontinuity for integer number of electrons, it is not possible to exactly evaluate this quantity.[66] However, it is possible to evaluate the chemical potential from either side of this discontinuity. This is equivalent to a situation in which the molecule either loses electron (μ^-), or gains one (μ^+). At zero temperature, these are exactly the ionization potential $I$and the electron affinity A, respectively. By considering $I = E(N) - E(N-1)$ and $A = E(N+1) - E(N)$, we can define the Fukui function for the molecule when either losing or accepting an electron, as the difference in electron density $\rho(r)$ in the two states (at the same molecular geometry):

$$\begin{aligned} f^-(r) &= \rho_N(r) - \rho_{N-1}(r) \\ f^+(r) &= \rho_{N+1}(r) - \rho_N(r) \end{aligned} \quad \text{(Equation 2)}$$

This now assumes a distinct chemical meaning, with $f^-(r)$ corresponding to the capability of losing an electron, and $f^+(r)$ of gaining one, which are both immediately identifiable with the nucleophilic or electrophilic character of a molecule, respectively. One last step involves the discretization[67] of the Fukui function in atomic contributions based on a Mulliken population analysis. The condensed Fukui function on the atom k is defined as:

$$\begin{aligned} f_k^- &= q_k(N-1) - q_k(N) \\ f_k^+ &= q_k(N) - q_k(N+1) \end{aligned} \quad \text{(Equation 3)}$$

where q_k is the Mulliken atom charge of atom k, calculated either in the neutral state with N electrons, or in the positively/negatively charged molecule ($N-1/N+1$ electrons). Note that the sign is inverted with respect to the corresponding continuous Fukui functions, as we are considering electrons bearing a negative charge. The Fukui functions were evaluated by carrying out a single-point calculation on the ground state geometry, first considering the neutral system and then considering it as singly charged, in a doublet state (one unpaired electron). The condensed Fukui function was then calculated as the difference between the Mulliken atom charge in the two conditions, for the atoms of interest.

TD-DFT calculations for single complexes were carried out with CAM-B3LYP[68,69] exchange-correlation functionals considering the first 200 electronic transitions. Functional systematically underestimate the λ_{max}.[70] For this reason, a shift of 0.8 eV is applied to the simulated spectra of $Al(meac)_3$, $Al(sal)_3$ and $Al(naphthal)_3$, while a 0.66 eV is applied to $Eu(hfa)_3$. These shifts are equivalent to a maximum error below 15% with respect to the experimental values, in line with the best values (around 18%) reported in the literature for aromatic systems.[71] Any attempts to simulate the absorption spectra of $[Eu(hfac)_3Al(L)_3]$ heterometallic complexes failed.

Synthesis of $[Ln(hfac)_3Al(meac)_3]$ (Ln^{3+}= Eu^{3+}, Gd^{3+}, and Tb^{3+})

The synthesis of the europium derivative $[Eu(hfac)_3Al(meac)_3]$ (**1Eu**) is described at length. **[Eu(hfac)3Al(meac)3] (1Eu)**: $[Al(meac)_3]$ (0.225 g; 0.61 mmol) was added to a colorless suspension of $[Eu(hfac)_3]$ (0.468 g; 0.61 mmol) in toluene (30 mL). The system was maintained under stirring at room temperature for 4h obtaining a pale-yellow solution which was taken to dryness under reduced pressure. The resulting colorless solid was dissolved in hot heptane and recrystallized cooling the solution at −20 °C. The crystalline solid was filtered and dried *in vacuo* for 6 h (0.402 g, 62.3% yield). Elemental analysis calculated for $[Eu(hfac)_3Al(meac)_3]$

($C_{30}H_{24}AlEuF_{18}O_{12}$): C 30.6%, H 2.2%; found C 30.6%, H 2.1%. ATR-IR (1700–650 cm^{-1}): 1654 (m), 1640 (w), 1615 (m), 1596 (m), 1547 (m), 1488 (m), 1435 (w), 1415 (w), 1370 (w), 1327 (m), 1300 (s), 1250 (s), 1200 (s), 1140 (s), 1101 (m), 1065 (m), 1017 (w), 1004 (w), 982 (w), 951 (w), 920 (w), 796 (s), 740 (w), 660 (s). ^{1}H NMR (C_6D_6): 7.88 (s, 3H, H_a), 4.39 (s, 3H, H_b), 4.16 (s, 9H, H_c),−1.98 (s, 9H, H_d); ^{19}F NMR:−79.37 (F). Single crystals suitable for X-ray analysis were obtained cooling a heptane solution of **1Eu** to −20 °C. Unit cell parameters: monoclinic, $P2_1/c$, a = 18.1954(5) Å, b = 11.8768(3) Å, c = 20.9424(6) Å, β = 98.4140(10)° V = 4477.0(2) $Å^3$.

[Gd(hfac)$_3$Al(meac)$_3$] (1Gd)

[Gd(hfac)$_3$] (0.474 g, 0.61 mmol) and [Al(meac)$_3$] (0.238 g, 0.61 mmol) in toluene (25 mL).[Gd(hfac)$_3$Al(meac)$_3$] (0.504 g, 68.0% yield). Elemental analysis calculated for [Gd(hfac)$_3$Al(meac)$_3$] ($C_{30}H_{24}AlF_{18}GdO_{12}$): C 31.3%, H 2.1%; found C 31.1%, H 2.0%. ATR-IR (1700–650 cm^{-1}): 1653 (m), 1640 (w), 1614 (m), 1598 (m), 1556 (m), 1542 (m), 1489 (w), 1416 (w), 1371 (w), 1327 (m), 1300 (s), 1250 (s), 1195 (s), 1137 (s), 1101 (m), 1065 (m), 1018 (w), 1004 (w), 981 (w), 952 (w), 920 (w), 797 (s), 740 (w), 659 (s). Single crystals suitable for X-ray analysis were obtained cooling a heptane solution of **1Gd** to −20 °C. Unit cell parameters: monoclinic, $P2_1/c$, a = 18.194(3) Å, b = 11.8784(11) Å, c = 20.934(2) Å, β = 98.552(11)° V = 4473.8(8) $Å^3$.

[Tb(hfac)$_3$Al(meac)$_3$] (1Tb)

[Tb(hfac)$_3$] (0.269 g, 0.35 mmol) and [Al(meac)$_3$] (0.130 g, 0.35 mmol) in toluene (40 mL).[Tb(hfac)$_3$Al(meac)$_3$] (0.264 g, 66.8% yield). Elemental analysis calculated for [Tb(hfac)$_3$Al(meac)$_3$] ($C_{30}H_{24}AlF_{18}O_{12}Tb$): C 31.0%, H 2.0%; found C 31.3%, H 2.1%. ATR-IR (1700–650 cm^{-1}): 1652 (m), 1641 (w), 1615 (m), 1597 (m), 1556 (m), 1542 (m), 1490 (w), 1415 (w), 1370 (w), 1327 (m), 1300 (s), 1250 (s), 1190 (s), 1137 (s), 1101 (m), 1065 (m), 1017 (w), 1004 (w), 982 (w), 951 (w), 920 (w), 796 (s), 740 (w), 660 (s).

Synthesis of [Ln(hfac)$_3$Al(sal)$_3$] (Ln^{3+}= Eu^{3+}, Gd^{3+}, and Tb^{3+})

The synthesis of the europium derivative **[Eu(hfac)$_3$Al(sal)$_3$]** (**2Eu**) is reported at length.[Al(sal)$_3$] (0.252 g, 0.65 mmol) was added to a colorless suspension of [Eu(hfac)$_3$] (0.504 g, 0.65 mmol) in toluene (35 mL) obtaining in few minutes a yellow solution. After 24 h of stirring the solution was taken to dryness under reduced pressure and the obtained yellow solid was dried *in vacuo* for 4 h (0.544 g, 72.4% yield). Elemental analysis calculated for [Eu(hfac)$_3$Al(sal)$_3$] ($C_{36}H_{18}AlEuF_{18}O_{12}$): C 35.2%, H 1.6%; found C 35.5%, H 1.5%. ATR-IR (1700–650 cm^{-1}): 1652 (w), 1617 (m), 1543 (m), 1524 (w), 1470 (m), 1453 (w), 1443 (w), 1407 (w), 1309 (w), 1250 (s), 1190 (m), 1140 (s), 1100 (m), 1027 (w), 948 (w), 904 (w), 867 (w), 796 (m), 754 (m), 740 (w), 670 (w), 658 (s). ^{1}H NMR (CD_2Cl_2): 11.01 (s, 3H, H_f), 7.12 (s, 3H, H_a), 7.16 (d, J_2= 7.3 Hz, 3H, H_e), 6.63 (t, J_2= 7.3 Hz, 3H, H_c), 5.83 (t, J_2= 6.3 Hz, 3H, H_d),−0.41 (d, J_2= 6.3 Hz, 3H, H_b); ^{19}F-NMR:−80.26 (F_a). Single crystals suitable for X-ray analysis were obtained from a hot heptane solution of **2Eu**. Unit cell parameters: monoclinic, C2/c, a = 40.737(4) Å, b = 11.5754(10) Å, c = 20.2469(19) Å, β = 113.375(3)° V = 8763.8(14) $Å^3$.

[Gd(hfac)$_3$Al(sal)$_3$] (2Gd)

[Gd(hfac)$_3$] (0.591 g, 0.76 mmol) and [Al(sal)$_3$] (0.297 g, 0.76 mmol) in toluene (25 mL).[Gd(hfac)$_3$Al(sal)$_3$] (0.684 g, 77.0% yield). Elemental analysis calculated for [Gd(hfac)$_3$Al(sal)$_3$] ($C_{36}H_{18}AlF_{18}GdO_{12}$): C 37.0%, H 1.6%; found C 37.1%, H 1.5%. ATR-IR (1700–650 cm^{-1}): 1652 (m), 1615 (m), 1543 (m), 1470 (m), 1454 (m), 1442 (m), 1407 (w), 1310 (w), 1250 (s), 1188 (m), 1139 (s), 1100 (s), 1028 (w), 951 (w), 903 (w), 868 (w), 796 (s), 754 (m), 739 (w), 669 (w), 659 (s). Single crystals suitable for X-ray analysis were obtained cooling a heptane solution of **2Gd** to −20 °C. Unit cell parameters: monoclinic, C2/c, a = 40.828(4) Å, b = 11.5732(8) Å, c = 20.271(2) Å, β = 113.384(9)° V = 8791.6(14) $Å^3$.

[Tb(hfac)$_3$Al(sal)$_3$] (2Tb)

[Tb(hfac)$_3$] (0.411 g, 0.53 mmol) and [Al(sal)$_3$] (0.210 g, 0.54 mmol) in toluene (40 mL).[Tb(hfac)$_3$Al(sal)$_3$] (0.323 g, 52.0% yield). Elemental analysis calculated for [Tb(hfac)$_3$Al(sal)$_3$] ($C_{36}H_{18}AlF_{18}O_{12}Tb$): C 37.0%, H 1.5%; found C 37.0%, H 1.5%. ATR-IR (1700–650 cm^{-1}): 1651 (m), 1616 (m), 1542 (m), 1470 (m), 1453 (m), 1443 (m), 1407 (w), 1310 (w), 1250 (s), 1190 (m), 1137 (s), 1100 (s), 1027 (w), 951 (w), 902 (w), 867 (w), 795 (s), 754 (m), 740 (w), 670 (w), 658 (s).

Synthesis of [Al(naphthal)$_3$]

Hnaphthal (1.820 g, 10.56 mmol) was added to a colourless solution of [Al(O^tBu)$_3$] (0.867 g, 3.52 mmol) in toluene (30 mL) obtaining an amber suspension which was refluxed for 4h. The precipitated yellow solid was filtered and dried *in vacuo* for 5 h (1.401g, 73.7% yield). Elemental analysis calculated for [Al(naphthal)$_3$]

($C_{33}H_{21}AlO_6$): Al 5.0%, C 73.3%, H 3.9%; found Al 5.4%, C 73.5%, H 3.7%. ATR-IR (1700–650 cm^{-1}): 1619 (m), 1605 (s), 1585 (m), 1542 (m), 1468 (w), 1431 (w), 1402 (w), 1391 (m), 1374 (s), 1343 (w), 1310 (w), 1196 (w), 1189 (w), 1163 (w), 1144 (w), 1099 (w), 984 (w), 939 (w), 864 (w), 831 (w), 770 (w), 746 (m), 658 (w). ^1H NMR ($CDCl_3$, fac +mer isomers): 9.91-9.85 (4s, 1H, CHO), 8.11 (t, 1H), 7.90-7.84 (d+dd, 1H), 7.67 (t, 1H), 7.57-7.51 (m, 1H), 7.37-7.33 (m, 1H), 6.98-6.91 (d+m, 1H). Single crystals suitable for X-ray analysis were obtained from diffusion of pentane vapors in a 1,2-dichloroethane solution of the product.

Synthesis of [Ln(hfac)$_3$Al(naphthal)$_3$] (Ln^{3+}= Eu^{3+}, Gd^{3+}, and Tb^{3+})

The synthesis of the europium derivative **[Eu(hfac)$_3$Al(naphthal)$_3$]** (**3Eu**) is described at length.[Al(naphthal)$_3$] (0.290 g, 0.54 mmol) was added to a colorless suspension of [Eu(hfac)$_3$] (0.420 g, 0.54 mmol) in toluene (50 mL) obtaining a dark yellow solution which was maintained under stirring for 24 h and then taken to dryness under reduced pressure. The yellow product was recrystallized from 20 mL of hot heptane and dried *in vacuo* for 5 h (0.412g, 58.0% yield). Elemental analysis calculated for [Eu(hfac)$_3$Al(naphthal)$_3$] ($C_{48}H_{24}AlEuF_{18}O_{12}$): C 43.9%, H 1.8%; found C 43.7%, H 1.6%. ATR-IR (1700–650 cm^{-1}): 1650 (m), 1620 (m), 1602 (m), 1586 (m), 1545 (m), 1459 (m), 1430 (m), 1420 (w), 1389 (m), 1368 (w), 1339 (w), 1305 (w), 1252 (s), 1197 (s), 1142 (s), 1101 (m), 982 (m), 951 (w), 840 (m), 799 (m), 774 (w), 750 (m), 659 (s). ^1H NMR ($CDCl_3$): 11.19 (s, 3H, H_h), 8.04 (s, 3H), 7.54 (s, 3H), 7.03 (s, 3H), 6.85 (s, 3H), 6.42 (s, 3H), 5.30 (s, 3H),−1,88 (s, 3H, H_b); ^{19}F NMR:−79.58 (F_a). Single crystals suitable for X-ray analysis were obtained from a heptane solution of **3Eu** at −20°C. Unit cell parameters: triclinic, $P\bar{1}$, a= 11.7127(15) Å, b= 13.9774(18) Å, c= 16.0940(22) Å, α= 89.799(5)°, β= 88.251(5)°, γ= 86.985(2)° V = 2629.92(9) Å^3.

[Gd(hfac)$_3$Al(naphthal)$_3$] (3Gd)

[Gd(hfac)$_3$] (0.457 g, 0.59 mmol) and [Al(naphthal)$_3$] (0.317 g, 0.59 mmol) in toluene (25 mL).[Gd(hfac)$_3$Al(naphthal)$_3$] (0.386 g, 52.3% yield). Elemental analysis calculated for [Gd(hfac)$_3$Al(naphthal)$_3$] ($C_{48}H_{24}AlF_{18}GdO_{12}$): C 43.7%, H 1.8%; found C 43.8%, H 1.7%. ATR-IR (1700–650 cm^{-1}): 1652 (m), 1620 (m), 1601 (m), 1586 (m), 1544 (m), 1459 (m), 1430 (m), 1420 (w), 1389 (m), 1368 (w), 1339 (w), 1306 (w), 1251 (s), 1196 (s), 1140 (s), 1101 (m), 982 (m), 950 (w), 840 (m), 799 (m), 774 (w), 750 (m), 659 (s). Single crystals suitable for X-ray analysis were obtained from a heptane solution of **3Gd**at −20°C. Unit cell parameters: triclinic, $P\bar{1}$, a= 11.4714(7) Å, b= 12.2361(8) Å, c= 18.8174(12) Å, α= 87.710(2)°, β= 85.916(2)°, γ= 86.082(2)° V = 2626.8(3) Å^3.

[Tb(hfac)$_3$Al(naphthal)$_3$] (3Tb)

[Tb(hfac)$_3$] (0.340 g, 0.44 mmol) and [Al(naphthal)$_3$] (0.236 g, 0.44 mmol) in toluene (25 mL).[Tb(hfac)$_3$Al(naphthal)$_3$] (0.416 g, 71.5% yield). Elemental analysis calculated for [Tb(hfac)$_3$Al(naphthal)$_3$] ($C_{48}H_{24}AlF_{18}O_{12}Tb$): C 43.7%, H 1.8%; found C 43.9%, H 1.9%. ATR-IR (1700–650 cm^{-1}): 1652 (m), 1620 (m), 1601 (m), 1585 (m), 1544 (m), 1459 (m), 1430 (m), 1419 (w), 1387 (m), 1367 (w), 1339 (w), 1307 (w), 1252 (s), 1198 (s), 1139 (s), 1100 (m), 983 (m), 951 (w), 840 (m), 799 (m), 774 (w), 750 (m), 660 (s).

X-Ray diffraction studies. Crystals of **1Eu, 2Eu, 3Gd** and [Al(naphthal)$_3$] were glued at the end of glass fibers ant their diffractions were studied at room temperature by means of a Bruker SMART Breeze CCD diffractometer equipped with graphite monochromated Mo-*Kα* radiation (*λ* = 0.71073 Å). The crystal data of all new compounds are listed in Table S1. Intensity data collections were carried out for all samples within a maximum 2*θ* of about 53 deg, because the diffractions besides this limit was very weak. All the structure solutions were found using the automated direct methods contained in SHELXS-97 program.[72] The crystal structure of **3Gd** contains cavities about 136 Å^3 wide in a ratio of 0.5 cavities per molecule. Although these cavities are virtually accessible to the solvent, they show no trace of electron density maxima. In order to exclude that the presence of a very disordered solvent could justify the absence of such maxima, the SQUEEZE procedure[73] was applied to the data. The fact that the calculation procedure converged to a value of only two electrons per cavity was considered sufficient to conclude that the cavities are empty. Some degree of disorder was present in the CF_3 groups of all four structures. The more disordered ones were considered distributed on two limit conformations. The structure refinement was done using SHELXL-97 program.[72] Reliability factors obtained in the final refinement cycles are listed in Table S1. Some other programs contained in WINGX[72] suite have been used in calculations. Supplementary crystallographic data for this paper have been deposited with The Cambridge Crystallographic Data Center and can be obtained free of charge from it. The deposition numbers for each compound are listed in Table S1.